A CLASSIFICATION SCHEME FOR LANDFALLING TROPICAL CYCLONES

BASED ON PRECIPITATION VARIABLES DERIVED FROM

GIS AND GROUND RADAR ANALYSIS

by

IAN J. COMSTOCK

JASON C. SENKBEIL, COMMITTEE CHAIR
DAVID M. BROMMER
JOE WEBER
P. GRADY DIXON

A THESIS

Submitted in partial fulfillment of the requirements
for the degree Master of Science
in the Department of Geography
in the graduate school of
The University of Alabama

TUSCALOOSA, ALABAMA

2011

ABSTRACT

Landfalling tropical cyclones present a multitude of hazards that threaten life and property to coastal and inland communities. These hazards are most commonly categorized by the Saffir-Simpson Hurricane Potential Disaster Scale. Currently, there is not a system or scale that categorizes tropical cyclones by precipitation and flooding, which is the primary cause of fatalities and property damage from landfalling tropical cyclones. This research compiles ground based radar data (Nexrad Level-III) in the U.S. and analyzes tropical cyclone precipitation data in a GIS platform. Twenty-six landfalling tropical cyclones from 1995 to 2008 are included in this research where they were classified using Cluster Analysis. Precipitation and storm variables used in classification include: rain shield area, convective precipitation area, rain shield decay, and storm forward speed. Results indicate six distinct groups of tropical cyclones based on these variables.

ACKNOWLEDGEMENTS

I would like to thank the faculty members I have been working with over the last year and a half on this project. I was able to present different aspects of this thesis at various conferences and for this I would like to thank Jason Senkbeil for keeping me ambitious and for his patience through the many hours spent deliberating over the enormous amounts of data generated from this research. I also thank David Brommer and Joe Weber for their service on my committee, and Grady Dixon, who traveled to Tuscaloosa from Starkville, MS for my defense, for his service as my external committee member.

CONTENTS

LIST OF TABLES

LIST OF FIGURES

1. Introduction

The Saffir-Simpson Hurricane Potential Damage Scale (Simpson 1974), renamed the Saffir-Simpson Hurricane Wind Scale (NOAA 2010) in 2010, is the most widely recognized hurricane classification scheme used in the Atlantic basin. It was devised by then National Hurricane Center (NHC) director Robert Simpson and a team of wind engineers to categorize the damage potential from hurricane force winds and flood potential from storm surge (Kantha 2006). It is an easily understood system with a 1 to 5 ranking of hurricane damage potential based on the maximum sustained wind speed (1 minute average at a height of 10 m, Powell and Reinhold 2007) of the hurricane (Table 1). The scale is most useful to coastal residents as a warning scale, prior to landfall, when residents must make a personal risk assessment; however, there are many hurricane hazards and variables neglected by the SS scale. Precipitation, a variable largely ignored in warning scales, is the primary focus of this thesis.

Table 1: The Saffir-Simpson Hurricane Wind Scale (revised 2010).

Category Strength	Maximum Wind Speed (ms^{-1})	Maximum Wind Speed (mph)
Tropical Storm	17 – 32	40 – 73
Hurricane Category 1	33 – 42	74 – 95
Hurricane Category 2	43 – 49	96 – 110
Hurricane Category 3	50 – 58	111 – 130
Hurricane Category 4	59 – 69	131 – 155
Hurricane Category 5	70+	156+

Despite its limitations in that it only accounts for one variable, the SS scale has undoubtedly spared the lives of numerous costal inhabitants. Hurricane fatalities are decreasing over time primarily because of mass evacuations of low-lying surge-prone areas. Vulnerable coastal populations evacuate to nearby states on the periphery of the storm, or they evacuate farther inland, albeit only to experience a weakened inland tropical cyclone (TC). Furthermore, populations in coastal counties, residing outside of hazardous surge zones, often choose to stay home unless the hurricane is forecasted to be catastrophic.

Thus, in either of these scenarios the vast majority of people are experiencing the decaying hurricane from an inland perspective as central pressure is increasing and winds are decreasing (Kaplan and DeMaria 1995). Research has shown that most fatalities from landfalling TCs in recent decades occurred inland due to flooding, often when a TC's maximum winds have weakened to below hurricane force (Rappaport 2000). With less emphasis on wind and surge at inland locations, the most hazardous threat is inland flooding (Rappaport 2000, Elsberry 2002, Negri et al. 2005).

Translational velocity (forward speed) of the storm is the primary determinant of the flooding potential of a landfalling TC. Slow-moving or stalled systems have been shown to be notorious flood producers (Camille 1969, Danny 1997, Georges 1998, Bonnie 1998, Floyd 1999). Due to the number of fatalities from inland flooding, it is important to gain a better understanding of less-obvious tropical cyclone precipitation characteristics in the post-landfall period. Recent research on TCs after landfall has shown that TC precipitation exhibits distinct characteristics in shape, intensity, and associations with the surrounding atmospheric environment (Marks and Houze 1987, Elsberry 2002, Atallah and Bosart 2003, Atallah et al. 2007, Matyas 2007). Matyas (2007, 2010) provides a spatial analysis of altered TC rain-shield shapes post-landfall. These studies are valuable contributions to the literature; however, they only tangentially approach the influence of tropical cyclone rain shield size upon the population experiencing the storm. A TC with a larger rain shield area (RSA) would theoretically have the potential to produce more flooding over a greater area when controlling for translational velocity. For this reason, analysis begins in this thesis by discussing variability in TC rain shield size before proceeding to other rain shield characteristics.

Another variable that exacerbates flooding potential is precipitation intensity. In this thesis, precipitation intensity is described as either stratiform (light intensity) or convective (heavy intensity). Convective precipitation area (CPA) is assessed as a size variable similar to RSA. Most convection and heavy precipitation is found within the inner core (storm center to 111 km radial distance) near the eye

(Marks 1985, Marks and Houze 1987, Cerveny and Newmann 2000, Cecil et al. 2002); however, many TCs contain bands of convective precipitation well removed from the center of the storm (Jorgensen 1984, Marks 1985). The majority of precipitation in TC rain shields is classified as stratiform (Jorgensen 1984); however, there is considerable variation between storms in the amount and intensity of precipitation that is classified as convective (Barnes and Stossmeister 1986, Burpee and Black 1989, Ryan et al. 1992, Ulbrich and Atlas 2002, Matyas 2009). There is also not a consistent relationship between RSA and CPA. It is possible to have several combinations of RSA and CPA. Thus, it is desirable to determine possible combinations of rain shield size and convective area that may contribute to flood potential.

TC rain shield size and convective area are influenced by many factors. Having a better understanding of the relationships controlling rapid or slow dissipation is a crucial determinant of flooding potential. Both variables eventually dissipate after landfall (Emanuel 2005); however, the rate of dissipation varies depending on the synoptic pattern, topographic features over which the storm passes, and ambient environmental parameters. Rapidly dissipating rain shields and smaller convective areas would theoretically be associated with reduced flooding potential. Ideally, observations of these precipitation variables could be summarized by a classification scheme analogous to the SS scale, albeit strictly using precipitation variables. The specific objectives of this thesis are listed below. The last objective (bold) is the primary goal.

- Discuss variability in tropical cyclone rain shield size and how it relates to precipitation.
- Analyze post-landfall expansion or dissipation of rain shield area.
- **Classify TCs into unique types based on their precipitation characteristics.**

This thesis proposes a classification scheme for landfalling tropical cyclones based solely on precipitation characteristics. The appellation given to the proposed scale is termed by the author as the Tropical Cyclone Precipitation Hazard Scale (TCPH). The TCPH scale attempts to categorize hurricanes by

variables that contribute to flood risk and total precipitation. It is a post-landfall assessment of TCs and, therefore does not apply to storms over open water, nor does it serve a functional operational purpose in its current form. Analogous to the HCS (Senkbeil and Sheridan 2006), it is an attempt to determine if flooding potential and precipitation hazards might be more appropriately assessed than methods that are currently available.

After much experimentation with variables, the proposed TCPH scale uses the size of the TC rain shield, precipitation intensity, and the translational velocity of the storm. Wind speeds and radii, as a size measure, are neglected in the TCPH scale as previous researchers have established only a weak correlation between the two (Merrill 1984), and alternative wind classification systems have been proposed by other TC researchers (Kantha 2006, Emanuel 2007, Powell and Reinhold 2007). The proposed TCPH scale serves to complement the SS scale, as well as other TC classification systems, as it is the only known classification scheme that isolates TC precipitation characteristics. When used in conjunction with other wind classification systems, the TCPH scale provides a more comprehensive understanding of the hazards associated with a landfalling TC.

2. Literature Review

a. The Tropical Cyclone

The tropical cyclone (TC) is defined by the American Meteorological Society as a closed circulation cyclone that originates in tropical latitudes (http://amsglossary.allenpress.com/glossary). When the maximum wind speed (V_{max}) of a TC attains 17.5 ms^{-1} (39 mph) the TC becomes designated as a tropical storm (TS) according to the Saffir-Simpson (SS) scale. When Vmax increases to 33 ms^{-1} (74 mph) the TC is referred to by its more common name (for Atlantic basin TCs), a hurricane. Nomenclature of tropical cyclones depends on the region of the earth in which it originated; Figure 1 is a map of formation regions and local terminology of TCs with hurricane force winds. TCs are the subject of much meteorological research; the succeeding paragraphs of this literature review detail the facets of TC research related to this thesis.

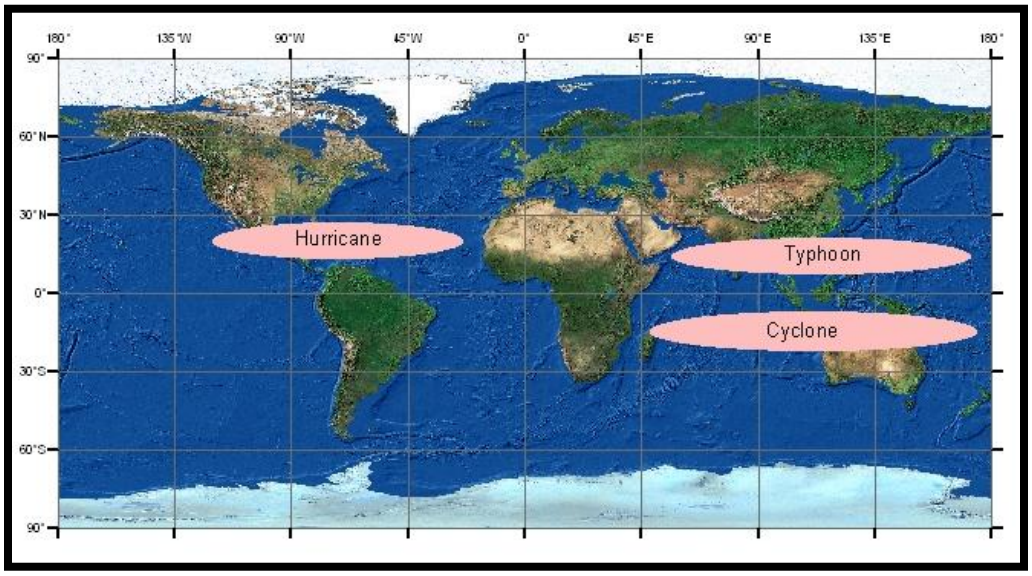

Figure 1: Worldwide nomenclature for tropical cyclone formation regions.

Inner and outer rainbands are described as being spiral in nature and displaced from the center of the storm but adjacent to the eyewall, with the outer bands extending radially as far as 200+ km (Maynard 1945, Marks 1985, Cecil et al. 2002). Rainbands are comprised mostly of stratiform precipitation however most of the accumulated rainfall from a TC is the result of convective precipitation (Jorgensen 1984, Marks 1985) due to the significantly higher rain rates of convective precipitation (3 – 30 mm h^{-1}) compared to stratiform rain (~0.5 mm h^{-1})(Jorgensen and Willis 1982). There is no defining limit as to how far the outer band extends from the TC center. Outer band precipitation is said by Cecil et al. (2002) to extend as far as can be subjectively attributable to the TC.

1) The TC Rain Shield

The area of precipitation associated with a TC is called the rain shield (Senn and Hiser 1959, Jorgensen 1984, Matyas 2007). Several distinct features are associated with rain shields and are typically readily visible in radar and satellite images. The center of the cyclone circulation is typically a rain-free, meteorologically tranquil eye (Maynard 1946), which usually ranges 10 – 50 km radially in size (Kimball and Mulekar 2004) and is most often found inside the radius of maximum winds (R_{max})(Shea and Gray 1973). The TC eye is a region of clear skies due to subsidence of the vertically moving air, which is sometimes referred to as the secondary circulation of the storm (Willoughby 1988, Emanuel 2003). Encompassing the eye is a "ring" of intense precipitation termed the eyewall; characteristics of the eyewall are discussed in the succeeding section on convective precipitation.

Most of the features discussed above are noted from observations of TCs monitored over open ocean water; these features are dramatically altered as a TC has a tendency to become asymmetric after landfall as the TC moves from a barotropic (lack of a horizontal temperature

gradient) tropical atmosphere into the more baroclinic middle latitudes. This is primarily the result of the interaction of the TC with features present over mid latitude land masses that are absent over the tropical oceans such as topography and terrain as well as synoptic-scale weather events (Marks and Houze 1987, Elsberry 2002, Atallah and Bosart 2003, Atallah et al. 2007, Matyas 2007).

2) Convective Precipitation

Convective precipitation falls from vertically developed cumulonimbus clouds sustained by updrafts with vertical velocities > 1 ms^{-1} that sometimes exceed 6 ms^{-1} (Barnes et al. 1983, Jorgensen 1984, Houze 1997). Convective precipitation associated with a TC is most prevalent in the eyewall, the intense convective precipitation that encircles the eye. A cross-sectional view of precipitation at radial distances from the eye of Hurricane Frederic (1979) is portrayed in Figure 3. Notice the large convective structure and enhanced reflectivities of the eyewall and also convective cells well removed from the center of the storm. Open-water measurements reveal that convection strength in a TC is typically weaker than thunderstorms encountered over land (Marks 1985, Cecil et al. 2002).

Convective precipitation is present in both the eyewall and rainbands, though convection in the eyewall tends to be more intense owing to stronger vertical motion than what is observed within convective cells of rainbands (Jorgensen 1984, Marks 1985, Marks and Houze 1987); though, as shown in Figure 2, convective precipitation has been observed at significant distances away from the storm center. Radar reflectivities are markedly higher under convective precipitation than reflectivity returns from stratiform rain. A discussion on radar reflectivity values of stratiform and convective precipitation is provided in the Methods chapter.

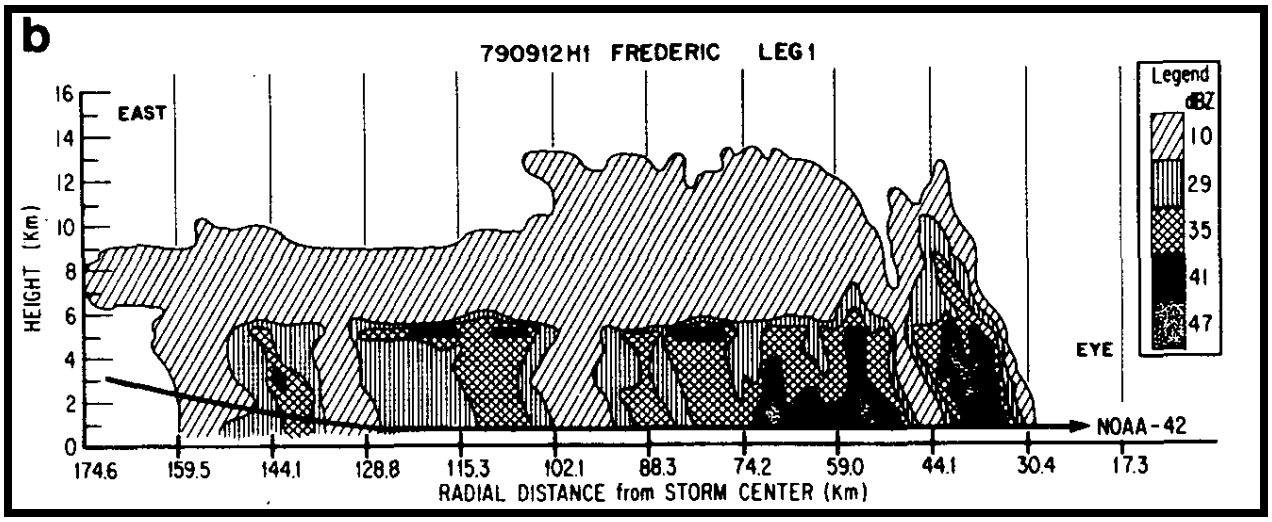

Figure 2: Cross section of hurricane Frederic (1979) showing the most intense convection near the eyewall, but also areas of intense convection well removed from the eyewall (from Jorgensen 1984).

3) The Importance of Translational Velocity on Rainfall

Translational velocity (storm forward speed) is currently not categorized and there is no standard threshold value as to what constitutes a slow TC, or how slow a TC needs to be to significantly heighten flood risk. TCs have a propensity to move along with the direction of prevailing winds (Willoughby 1999, Emanuel 2003) at forward speeds averaging 2 – 8 ms^{-1} (Weatherford and Gray 1988, Emanuel 2003). The translational velocity of a TC (or any heavy precipitation event) has major implications for flood potential. A slow moving TC increases the flood potential of a storm (Atallah et al. 2007, Medlin et al. 2007) regardless of its convective activity; however, it should be noted that flooding potential is also dependent upon several factors such as rain rate, antecedent environment, and local hydrologic conditions (Elsberry 2002).

b. TC Size

The size of a tropical cyclone is often described by its radius of the outer closed isobar (ROCI) or the radius of gale-force winds (17 ms^{-1}, Merrill 1984) (Figure 3). Merrill constructed a climatology of

TC size for north Atlantic and north Pacific TCs during 1957 – 1977, cataloging ROCI values (measured in degrees) for each basin. The results of that work show that most Atlantic TCs range 2° – 3° (latitude) in size while most Pacific TCs were slightly larger with the mode of ROCI values equating to 3° – 4° (latitude) in size. Merrill's results came from data provided by the National Hurricane Center's (NHC) Best Track dataset (Jarvinen and Caso 1978). Most modern determinations of hurricane size radii are now recorded in kilometers, rather than degrees (Bell and Ray 2004, Kimball and Mulekar 2004, Demuth et al. 2006, Moyer et al. 2007, Dean et al. 2009). Merrill also found no significant correlation between the maximum wind speeds (Vmax) of a TC in relation to its size.

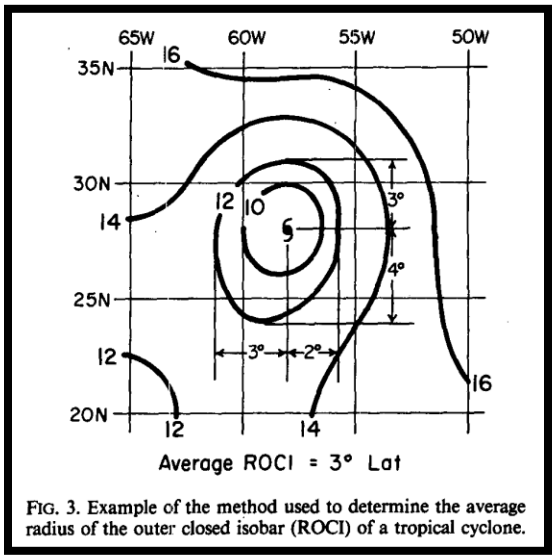

FIG. 3. Example of the method used to determine the average radius of the outer closed isobar (ROCI) of a tropical cyclone.

Figure 3: The determination of ROCI (from Merrill 1984).

Numerous studies on TC size have been conducted since the Merrill 1984 paper. Bell and Ray (2004) constructed a climatology of TC wind radii in the Atlantic basin for 1977–1999. They recorded the radius of hurricane-force winds (R_{hf}) and the radius of maximum winds (R_{max}) in multiple quadrants of thirty-three hurricanes partitioned by subjective determinations of major (sea

level minimum pressure < 965 mb) and minimal hurricanes (sea level minimum pressure $\geq$ 965 mb). Their study resulted in a predictive model for estimating the probability of R_{hf} occurring at a specific distance from storm center. The results of this model found that R_{hf} values of major hurricanes extend further radially from the TC center than minor hurricanes and R_{hf} values are more likely to occur in the right front quadrant of both major and minimal hurricanes. Dean et al. (2009) followed a similar approach as they derived statistical regressions to predict outer wind radii of 34-knot (17.5 ms^{-1}) winds and described their various statistical probability distributions.

Kimball and Mulekar (2004) constructed a climatology of north Atlantic TCs for 1988 – 2002. Their climatology was also a catalog of wind radii that included ROCI and eye measurements. Their climatology is fairly comprehensive and examines changes in size parameters through steady state (Vmax not changing), intensification (Vmax increasing), and weakening (Vmax decreasing) phases of the TC. Furthermore, the Kimball and Mulekar (2004) dataset provides a regional analysis and statistically analyzes TC size during the three phases of ENSO. The analysis of TC size in the Kimball and Mulekar (2004) climatology discontinues after Vmax falls below TS strength (17 ms^{-1}). Demuth et al. (2006) coalesced the methods of Bell and Ray, and Kimball and Mulekar by using the Advanced Microwave Sounding Unit on board several NOAA satellites to estimate the radii of 34-kt (17.5 ms^{-1}), 50-kt (26 ms^{-1}), and 64-kt (33 ms^{-1}) winds in four quadrants of a TC.

The aforementioned studies evaluate TC size almost exclusively when the TC is over open water. Little research has been done to summarize how TC size changes after landfall though much research has been done on how individual storms interact in a baroclinic environment (Bosart and Bartlo 1991, Bosart and Lackmann 1995, Atallah and Bosart 2003, Atallah et al. 2007, Arndt et al. 2009, Garlaneau et al. 2010). Estimating the size of TC rain shields after landfall is difficult because of the many complex interactions that take place between the TC and topography as well as the difficulty of partitioning TC precipitation from synoptic-scale precipitation events in the vicinity of

the cyclone. Qualitative statements about rain shield size were provided by Elsberry (2002) and Atallah et al. (2007). They found that rain shields tend to expand during extratropical transition (ET) when precipitation distribution shifts to the left of the cyclone track.

Matyas (2010) is the first known study to use GIS to formally apply quantitative measurements to rain shield size. Her analysis was primarily a predictive study of the radial extent of thirty-one TC rain shields at landfall in four quadrants centered about the circulation center (a method similar to Bell and Ray). She utilized control variables from the Statistical Hurricane Intensity Prediction Scheme dataset (DeMaria and Kaplan 1994, 1999, DeMaria et al. 2005) and found that TC rain shields are often enclosed by the ROCI.

The abovementioned studies make clear that TC size is an important variable to consider beyond wind and pressure radii. Maximum winds are typically confined to the cyclone's inner core (center to 111 km), though they have been shown to extend beyond 300 km (Kimball and Mulekar 2004); the rain shield extent has been shown by Matyas (2010) to (on average) extend beyond the inner core between 150 and 300 km, sometimes beyond 500 km.

c. Hurricane Hazards and Classification

1) Hazards and Risk Perception

Comprehending which hurricane hazards coastal residents find most threatening and finding what most influences evacuation decisions depends on a multitude of factors: government orders, distance from coastline, housing structure, family size, pet ownership, influence of neighbors, perception of home safety, past experience with storms, fear of looting, employment obligations, among many others (Baker 1991, Dow and Cutter 2000, Senkbeil et al. 2009). Studies of evacuation decision making can only come from respondents of surveys from those who have evacuated storms, which are irregular in occurrence, especially notably damaging

ones. Evacuation from Hurricane Rita (2005) was one of the most participatory ever, precipitated in large part by the catastrophe surrounding the events of Hurricane Katrina just one month prior (NHC Archives).

Baker (1991) identifies low-, moderate-, and high-risk coastal areas, based primarily on distance from the coastline and sea level elevation. Research in the last decade has revealed that flooding is the primary cause of loss of life in the U.S. from landfalling TCs (Rappaport 2000, Ellsberry 2002). Both of the previously cited studies were published before Hurricane Katrina (2005), arguably the most notorious natural disaster in the United States in several decades. The socio-economic impacts of Katrina are beyond the scope of this thesis, however the event did highlight the need for more public awareness of the threat of flooding from tropical cyclones, especially vulnerable populations living in low lying areas.

2) Classification

The SS scale has been in operational use for nearly forty years, though in recent years many propositions of alternative measures of TC classification have been published that incorporate aspects of TCs not present in the SS scale; many of these include elements of TC size into their damage potential measures. Storm surge was eliminated from the SS scale in 2010 as recent research has shown that storm surge is not adequately correlated to maximum wind speeds. Irish et al. (2008) showed that storm surge is better correlated to TC size (as defined by the R_{max}) rather than maximum wind speeds. With the omission of surge classification, maximum wind speed is the sole basis of tropical cyclone classification for the leading hurricane classification scale and surge forecasts are now issued on an individual basis (NOAA 2010). The events surrounding Hurricane Katrina in 2005, a category 3 hurricane (at landfall) according to the SS scale, have likely precipitated much of the debate as to the adequacy of the SS scale to estimate

TC damage potential. Many alternatives to the SS scale include indices rather than distinct categories with absolute categorical value limits (Kantha 2006, Emanuel 2007, Powell and Reinhold 2007). Kantha stated that differences in wind damage potential between wind speeds teetering on category boundaries are minor. He proposed the Hurricane Intensity Index which divides Vmax by 33 ms^{-1} and squares the result $\left(\frac{\text{Vmax}}{\text{Vmax}_0}\right)^2$. He also proposed a more complex, Hurricane Hazard Index, which incorporates Vmax, R_{max}, and storm forward speed. Jordan and Clayson (2008) provide a critique of Kantha's alternative indices. Powell and Reinhold proposed an intricate mathematical index which they named as Integrated Kinetic Energy (IKE). IKE is conceptually straightforward yet quite complex mathematically. Rather than accounting for size in one lateral dimension, IKE integrates wind speeds over a volume of airspace.

Senkbeil and Sheridan (2006) conglomerated wind speed, forward motion, and observed rainfall into their Hurricane Classification System (HCS). The HCS is a post-landfall analysis with a categorical index similar to the SS scale, but without distinct categorical boundaries. This is possibly the first classification scale that attempts to incorporate precipitation into a categorical system. Several TC parameters are evaluated (pressure, wind speed and gusts, surge, duration, and accumulated rainfall) and rated on a scale that assesses storm speed to storm intensity.

Intricate and comprehensive classification systems such as Emanuel's Power Dissipation Index and Integrated Potential Kinetic Energy by Powell and Reinhold are useful for scientists evaluating complex features integral to estimating damage potential and improving damage estimation techniques, though they can be difficult for non scientists to comprehend. When tropical cyclogenesis occurs, the information available to the public becomes overwhelmingly abundant, especially with the wealth of information available from local media, twenty-four hour news networks, and the internet. The SS scale is a condensed and simplistic categorical scheme that most media outlets will use to summarize the storm. There is no doubt however

that part of the reason for its longevity is its simplistic nature, which paradoxically can lead to misunderstandings of the storm. The desired effect of a classification system is to be simple enough for non scientists to understand, yet comprehensive enough that meaningful generalizations can be made from the scale.

3) Probability of TC Landfalls

This research deals exclusively with hurricanes that have made landfall in the U.S. Though not the focus of this research, it seems that a short discussion on hurricane landfall probability is appropriate. The El Niño Southern Oscillation (ENSO) is a teleconnection index that has a prominent influence on U.S. landfall frequency. ENSO is typically described as having three phases: a warm phase where east/central Pacific sea surface temperature (SST) is substantially above normal causing an El Niño event, a cool phase which is the reverse of the warm phase and deemed a La Niña event, and ENSO neutral which represents normal or average conditions (Kiladis and van Loon 1988, Trenberth 1997). Hurricane formations and landfalls tend to dominate during La Niña events (Gray 1984, Bove et al. 1998, Goldenberg et al. 2001, Smith et al. 2007) as atmospheric conditions favorable to tropical development are more prevalent during the cold phase of ENSO (Gray 1984, Goldenberg et al. 2001). The landfall probability in the United States during the three ENSO cycles is presented in Figure 5. It is apparent from Figure 4 that hurricane landfalls are most likely during cold ENSO, and warm ENSO cycles have the lowest TC landfall probability in the U.S. A more detailed analysis of hurricane landfalls can be found in (Gray et al. 1994, Elsner and Bossak 2001, Brettschneider 2008).

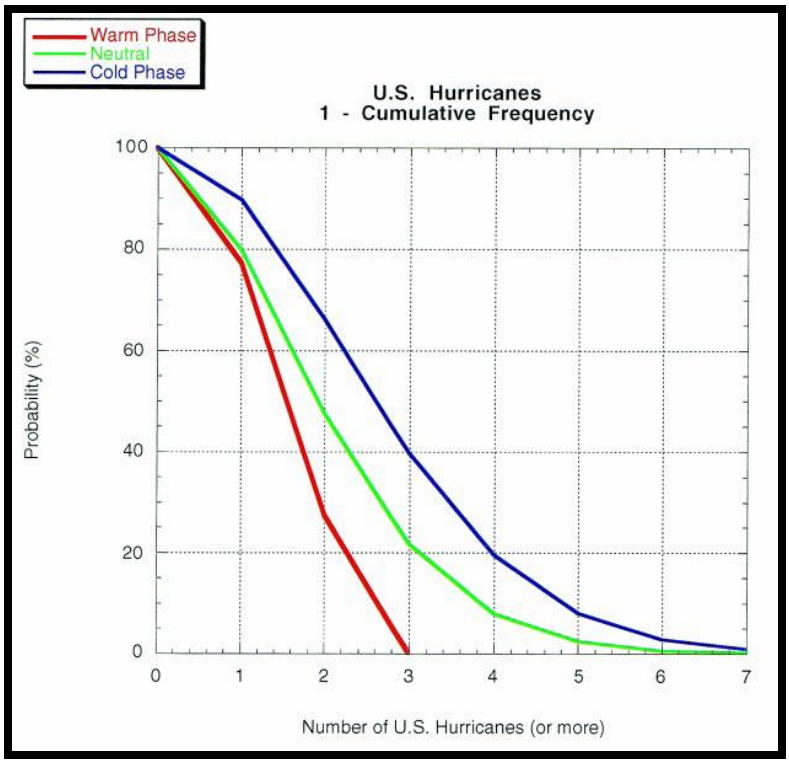

Figure 4: Cumulative frequency diagram indicating the probability of number of U.S. landfalls during the three phases of ENSO.

3. Methods

a. Storm Selection

Twenty land-falling hurricanes and six tropical storms are included in this thesis. Storm selection is limited to TCs during or after the 1995 hurricane season as GIS data for WSR-88D sites are not available prior to 1995 (Ansari and Del Greco 2005). TCs are large atmospheric phenomena whose horizontal extents are rarely captured by a single radar facility; therefore, each TC must have adequate radar coverage available for each time-step to be included in analysis. Several TCs made landfall in the U.S. after the 1995 season that were not included in this analysis for lack of adequate radar coverage. Furthermore, each radar facility used to capture each TC must provide coverage of the storm for each time step. If a radar facility did not provide coverage of the storm for each of the three periods, the facility was excluded from analysis. Each land-falling TC in this study is included in Table 2. TC tracks were downloaded online from NOAA's Coastal Services Center (http://www.csc.noaa.gov). Tracks were used only to indicate the path of each TC. Tracks were used to discuss the relevance of landfall location to damage incurred from a land-falling TC.

b. Data

1) Radar

Base reflectivity from the Weather Surveillance Radar (WSR-88D) was used for all TC rain shields in this thesis. Details on the location and elevation of each radar facility can be found in Appendix A. The WSR-88D radar can detect reflectivities out to 460 km (Crum and Alberty 1993), though only phenomena with very large vertical profiles such as TCs can be detected at such distances (Willoughby 1999). This range may also be limited by the "ducting" effect resulting from the high temperature, high vapor pressure, and low atmospheric pressure present in a tropical cyclone (Federal Meteorological Handbook 2005). Analysis begins at

landfall due to uncertainties in the ability to detect the entire rain-shield in the hours before a TC crosses the coastline.

Long-Range Level –III Base Reflectivity shapefiles were downloaded via NOAA's HDSS Access System (HAS) (http://www.ncdc.noaa.gov/nexradinv/). Level-II data generally have better spatial resolution but presented two problems for this research: Level-II radar data was not as widely available as Level-III data and the file sizes of Level-II data were prohibitively larger than the Level-III data. Level-II data was available for many storms but it was not desired to mix Level-II shapefile polygons with Level-III shapefile polygons; in the interest of consistency, only Level-III shapefile polygons were used.

Rainfall estimation via radar serves as a means to substantiate the results of this study; however, each of the various methods of rainfall measurement has its inherent errors. Rainfall measurements (via rain gauge, radar estimation, and/ or reanalysis data) are used for comparisons between TCs and groups of TCs (obtained in the results of this thesis) though rainfall estimation data was not used in any of the statistical analyses of this thesis. Reanalysis data from NOAA's National Center for Environmental Prediction (NCEP) were obtained online from http://www.esrl.noaa.gov/psd/data/composites/hour/ (Kalnay et al. 1996). Daily composite images of precipitation rate (mm/ day) were obtained for each TC on the day of landfall. If the TC made landfall between 1201Z and 2359Z, the twelve hour study period would span two days and thus the composite images were averaged over two days.

Table 2: List of all Twenty-six tropical cyclones used in this thesis.

Name	Landfall Date	Saffir-Simpson Cat.
Erin	02-Aug-95	1
Bertha	12-Jul-96	2
Danny	18-Jul-97	1
Earl	03-Sep-98	1
Georges	28-Sep-98	2
Bret	23-Aug-99	3
TS_Helene	22-Sep-00	TS
TS_Allison	05-Jun-01	TS
Isidore	26-Sep-02	TS
TS_Bill	30-Jun-03	TS
Claudette	15-Jul-03	1
Isabel	18-Sep-03	2
TS_Bonnie	12-Aug-04	TS
Charley	13-Aug-04	4
Gaston	29-Aug-04	1
Frances	05-Sep-04	2
Ivan	16-Sep-04	3
Jeanne	26-Sep-04	3
Dennis	10-Jul-05	3
Katrina	29-Aug-05	3
Rita	24-Sep-05	3
Wilma	24-Oct-05	3
Humberto	13-Sep-07	1
Dolly	23-Jul-08	1
TS_Fay	19-Aug-08	TS
Gustav	01-Sep-08	2
Ike	13-Sep-08	2

2) National Hurricane Center Best Track and Extended Best Track Datasets

Information on landfall location, date and time, and maximum sustained winds (Vmax) were obtained from the National Hurricane Center (NHC) Archive of Hurricane Seasons (available online from http://www.nhc.noaa.gov/pastall.shtml). TC size parameters archived by the NHC were obtained from the Extended Best Track (EBT) dataset (Demuth et al. 2006) which is also available online (http://rammb.cira.colostate.edu/research/tropical_cyclones/tc_extended_best_track_dataset/). The best track and EBT datasets record observations at six-hour regular intervals (00Z, 06Z, 12Z, and 18Z), and best track data also provides information for the landfall of each TC. This research records data at six hour intervals as well, however the intervals begin at landfall (according to NHC Best Track data) and therefore values for the variables from the Best Track and EBT data are interpolated linearly to correspond with landfall (t_0), and six hours (t_{+6}) and twelve hours (t_{+12}) post-landfall.

3) TC Tracks

TC tracks were downloaded online from NOAA's Coastal Services Center (http://www.csc.noaa.gov). Tracks were used only to indicate the path of each TC. Tracks were used to discuss the relevance of landfall location to damage incurred from a landfalling TC.

4) Metadata

All metadata from the GIS data used in this research are available online through NOAA's National Climatic Data Center (NCDC). The NCDC website (http://www.ncdc.noaa.gov) houses metadata for all NOAA geospatial resources (http://www.ncdc.noaa.gov/oa/metadata/metadataresources.html). Metadata for each radar

site where digital WSR-88D data were downloaded from are available from NOAA's Multi-Network Metadata System (https://mi3.ncdc.noaa.gov//mi3qry/search.cfm). Metadata for TC tracks downloaded from the Coastal Services Center can be downloaded from http://www.csc.noaa.gov/metadata/.

c. GIS Analysis

Radar images were composited by mosaicing single-sweep radar scans of facilities providing coverage of each TC. In this research, the outer boundary of stratiform precipitation for each storm was delimited to contiguous precipitation with radar reflectivity values $\geq$ 20 dBZ. A value of 20 dBZ was chosen as the lower limit of radar reflectivity to define the outer edge of the outer rainband for each TC. A value of 20 dBZ has been used in previous studies to identify the outer edge of TC precipitation (Jorgensen 1984, Willoughby 1988, Cecil 2002, Matyas 2007). A value of 25 dBZ has been used extensively in previous research as the definition of the outer edge of TC precipitation as well (Barnes et al. 1983, Marks 1985, Barnes and Stossmesister 1986, Cecil et al. 2002). Matyas (2007) found that using 20 dBZ resulted in less fragmented precipitation bands; hence 20 dBZ was chosen as the lower limit of reflectivity rather than 25 dBZ. The demarcation of fragmented precipitation and "feeder bands" and from precipitation influenced from synoptic systems becomes increasingly difficult at greater distances from the TC center. Precipitation boundaries of TCs are not as clearly identifiable compared to wind speed and pressure boundaries. Consequently some degree of subjectivity is unavoidable when assessing the size of the TC rain shield over land. The highest reflectivity values are retained over areas where radar coverage of the TC overlaps between more than one facility. This was accomplished through multiple union computations as each radar facility for each TC was added individually. The code written for this procedure is available in Appendix B. Figure 5 depicts Hurricane Isabel (2003) at landfall with each WSR-88D facility

contributing data represented. Also shown in Figure 5 is the interpolated ROCI (dashed ring) centered about the circulation center. Reflectivity values are delineated every 5 dBZ for each radar sweep imported into the GIS. Color coding for display in the Data Frame was also accomplished via an ArcObjects program, written in Visual Basic, which is detailed in Appendix B. The Calculate Areas function computes the area of each individual polygon in a selected shapefile. After all radar shapefiles were mosaiced into a single shapefile representing the entire rain shield, the Calculate Areas function was run on the mosaiced shapefile. Precipitation area variables were computed in the GIS by summing the individual polygons of radar reflectivity from each mosaiced layer according to their dBZ value. Total storm area was computed by adding the areas of all of the polygons $\geq$ 20 dBZ. Jorgensen (1984) expressed the difficulty in accurately measuring the areas of asymmetrical TC rain shields. The spatial computational ability of GIS platforms allows for such calculations to be made quite accurately and efficiently. Measuring the rain shield area also eliminates the need to make radial measurements in multiple quadrants of a TC when size, rather than shape and asymmetry, is of primary concern. A flow chart of the data collection and processing is depicted in Figure 6.

The Weather and Climate Toolkit (Ansari and Del Greco, 2005), available online at http://www.ncdc.noaa.gov/oa/wct/index.php, was used to georeference shapefiles downloaded from the NEXRAD HAS. Georeferencing attaches spatial attributes (coordinates) to the radar reflectivity polygons, which allow them to be imported into the GIS and assigned to an appropriate coordinate system. The Albers Equal Area projection was the only projection used as it preserves size at the expense of shapes and angles. The utility of GIS in this research is its ability to efficiently compute TC size.

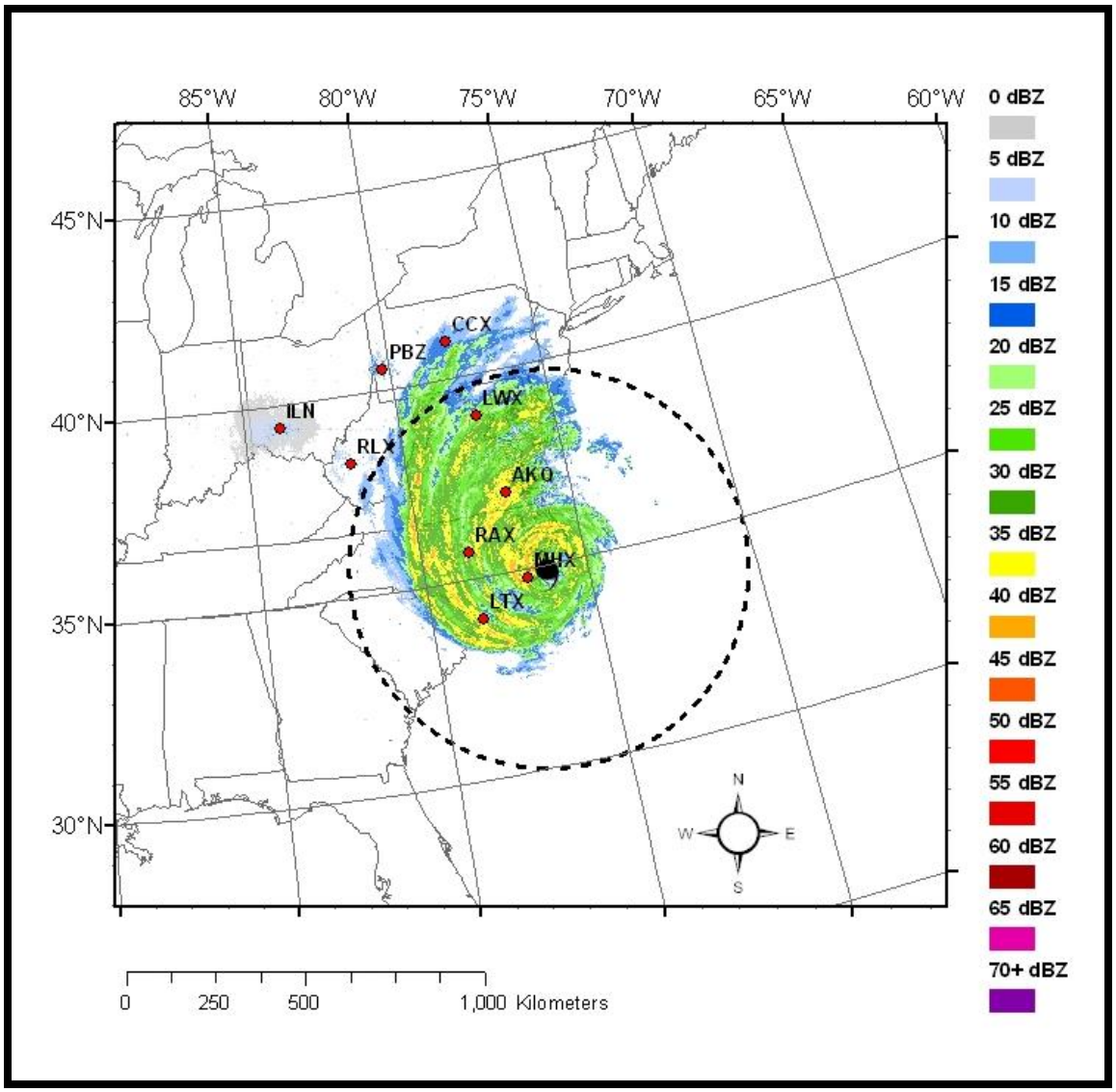

Figure 5: GIS composited image of Hurricane Isabel (2003) depicting each radar facility from which Level-III WSR-88D data was used to create the image.

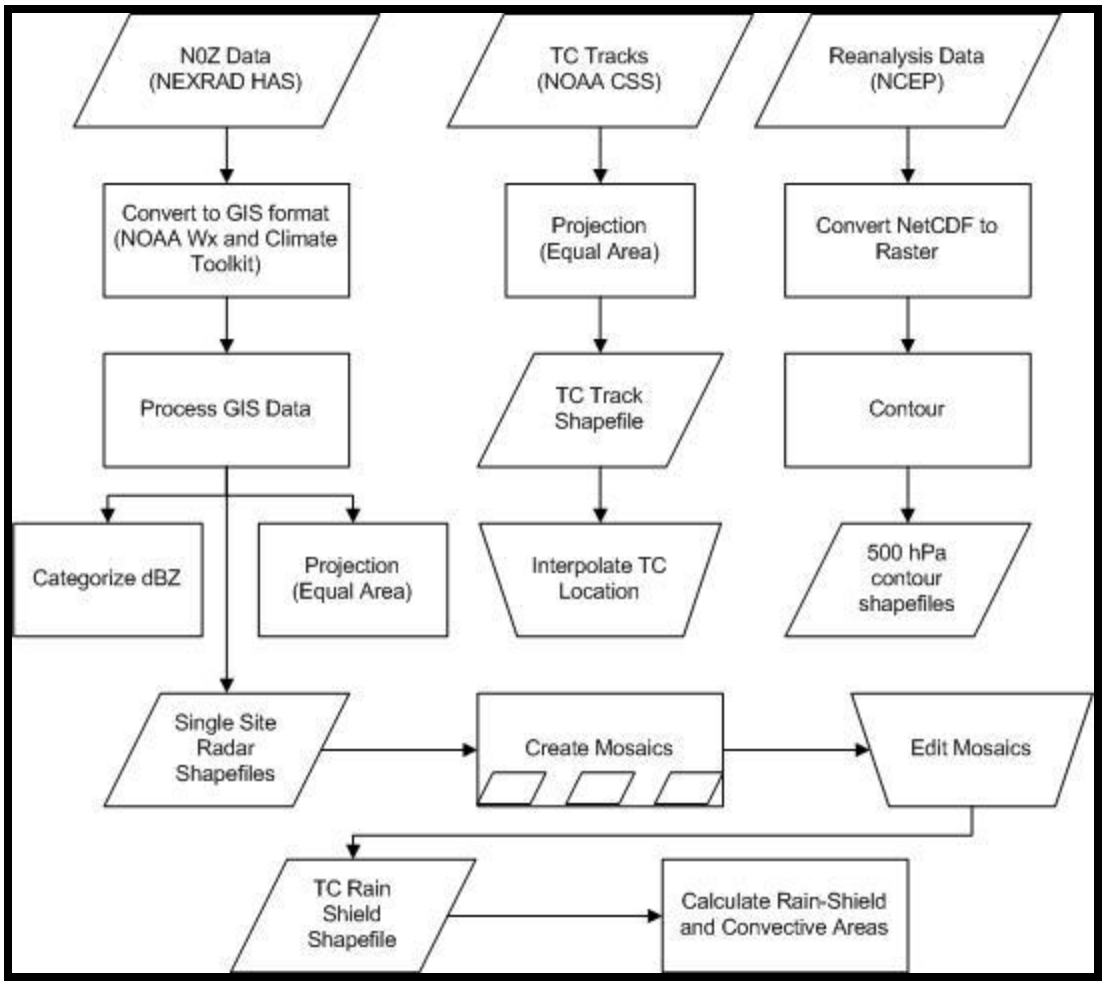

Figure 6: Flow chart depicting the data collection and processing of data used in this thesis.

d. Stratiform and Convective Precipitation

Numerous studies have been carried out describing methods to classify TC precipitation as either convective or stratiform (Barnes et al. 1983, Jorgensen 1984, Steiner et al. 1995, Houze 1997, Ulbrich and Atlas 2002, Matyas 2009). For landfalling TCs, horizontal radar reflectivity from ground-based radar (WSR-88D) is most appropriate for partitioning stratiform and convective type precipitation (Steiner et al. 1995). When using radar reflectivity, detection of the bright band is an explicit way to identify regions of stratiform rain. It is impractical however to use bright band identification from ground based radar as a sole means for stratiform precipitation identification. The vertical resolution of the radar at long range is often too coarse to pick up the bright band at the storm's periphery (Houze 1997), and the nonexistence of a bright band does not imply convective precipitation. If bright band identification was used alone to demarcate stratiform precipitation from convective precipitation, an excessive estimate of convection would occur (Steiner et al. 1995, Houze 1997). A value of 40 dBZ is too intense to be stratiform (Steiner et al. 1995), therefore all polygons $\geq$ 40 dBZ in this paper are classified as convective. Some studies have identified reflectivity vales < 40 dBZ that may be convective (Barnes and Stossmeister 1986, Burpee and Black 1989, Matyas 2009). A value of 20 dBZ corresponds to light rain when using base reflectivity data and is used as the lower limit of stratiform precipitation. Each TC shapefile contained 100,000 – 300,000+ polygons and, therefore, an ArcObjects program was written by the author to add 20+ dBZ and 40+ dBZ reflectivities, yielding separate measurements for total storm area (stratiform + convective precipitation) and convective precipitation only. The program code is listed in Appendix B.

Radar mosaiced images are indicative of the reflectivity at the moment of the scan, and images were not time-averaged. Open-water measurements of TCs have shown that convective cells tend to be highly variable, changing in size and intensity on short time scales often less than one hour (Lewis and Jorgensen 1978, Barnes and Stossmeister 1986, Barnes et al. 1991). Convective

precipitation measured from the composited images represents the area extent of precipitation at the particular time of the radar scan, and temporal results of TC overland convection can be more variable from the results presented in this thesis.

e. Statistical Analysis

TCs in this dataset were classified using cluster analysis in SPSS. The initial dataset in this research was comprised of a large array of TC rain shield variables. In developing the classification scheme for this thesis, the need for data reduction was apparent. This was attempted through Principal Components Analysis (PCA). PCA was intended to reduce all variables into discrete orthogonal groups that capture and explain the greatest amount of variance from the original variables. Although, several attempts were made with different combinations of variables, PCA was unsuccessful due to a fairly small sample size and a lack of significant correlations among the original variables. Thus, the original variables were used in cluster analysis procedures.

Four of the original variables were used for Cluster Analysis procedures. These variables are:

- Rain Shield Area
- Convective Precipitation Area
- Change in rain shield area between t_0 and t_{+12}
- Average translational velocity between t_0 and t_{+12}

Two variables, total rain shield area at landfall and the change in rain shield area between t_0 and t_{+12}, are included to account for TC size while total TC convective area and average translational velocity (between t_0 and t_{+12}) give insight into precipitation intensity and the flooding potential of the TC. An explanation of each variable and the rationale for their inclusion in this classification scheme is discussed in the Results chapter. Cluster analysis was a two-step process. Hierarchal

Cluster Analysis (HCA) was used to determine the ideal number of clusters (categories) while K-means Cluster Analysis (KCA) was used to assign TCs to individual clusters.

Both clustering procedures have a tendency to weight variables with larger magnitudes more than variables of smaller magnitudes. Variables with relatively large magnitudes (such as RSA) and comparatively small differences between cases (TCs) will register larger between-case differences than variables with relatively small magnitudes (such as translational velocity), and will therefore tend to group TCs by the larger-magnitude variables with little regard given to smaller-magnitude variables. This effect is mitigated by standardizing each variable. Normalization of all variables was performed by a simple Z-score calculation for all variables used in the classification scheme:

$$z = \frac{x - \bar{x}}{s} \tag{1}$$

where x = observed raw value for selected variable, $\bar{x}$ = mean of selected variable (between the twenty-six TCs), and s = standard deviation of selected variable. This ensured equal weighting of each variable in the classification and thus applied equal importance to each. This decision was subjective and the argument is open as to which variables may present larger threats to TC flooding over other variables.

1) Hierarchal Clustering

Initially, HCA was used as a guideline to determine the number of clusters to be used in the proposed classification. SPSS defaults were used for the computational methods of HCA. Similarity measurements were determined through Euclidean distance (d):

f. $$d_{ij} = \sqrt{\sum_{k=1}^{p} \left(x_{ik} - x_{jk}\right)^2} \tag{2}$$

where i = variable 1, j = variable 2, k = variable order (TC #1, #2, #3, …Bertha, Claudette, Earl, etc), and p = number of variables (26 TCs). An example of similarity between RSA and CPA is

presented follows: Hurricanes Isabel and Isidore were rather large TCs while Hurricanes Danny and Bret were quite small as defined by their rain shield areas. The total similarity (between the four variables) between the two large and two small TCs is calculated as follows:

$$d_{Isisore,Isabel} = \sqrt{(2.35 - 2.23)^2 + \left(-0.96 - (-1.78)\right)^2 + \left(-0.48 - (-0.56)\right)^2 + (0.73 - 1.26)^2} = 1.55$$

$$d_{Danny,Bret} = \sqrt{\left(-1.51 - (-1.27)\right)^2 + (0.27 - 0.45)^2 + \left(-1.69 - (1.76)\right)^2 + \left(-2.001(-1.24)\right)^2} = 1.25$$

The above calculations show that the Euclidean distances between the two pairs are similar to each other, however when the large TCs are compared to the small TCs noticeable changes are prevalent: $d_{Isidore,\ Danny} = 9.03$, $d_{Isidore,\ Bret} = 8.28$, $d_{Isabel,\ Danny} = 10.19$, $d_{Isabel,\ Bret} = 9.43$. It is inferred from the previous calculations that across the four TC variables (rain shield area, change in rain shield area, convective area, and average forward speed), hurricanes Isidore and Isabel are most similar to each other while Hurricanes Danny and Bret are also similar to each other (Isidore and Bret, and Isabel and Danny are the most dissimilar TCs in the example).

2) K-Means Clustering

K-means clustering was used to determine the final output groups based on the input of HCA. Unlike HCA, the number of groups in K-means needs to be predetermined before cases can be assigned to groups (this was accomplished with HCA). Like HCA, KCA is sensitive to outliers in datasets though the clustering algorithms are different between the two methods. An example of KCA clustering is shown in Figure 7. The example shows the clustering of two-dimensional data with five group centers (obtained online from http://cs.cmu.edu/~dpelleg/kmeans-images/f9.gif). The data in this thesis is four dimensional and thus is not illustrated easily. Group membership is based on distance of cases (tropical

cyclones in this research) from group centers, and group means are moved through multiple iterations to minimize the distance between case values and group centers. Unlike HCA, KCA runs multiple iterations where cluster membership can change, whereas, in HCA, once a case (TC) has been assigned to a group, it remains in the cluster. KCA has a tendency to determine outlying data as group centers, and assigns cases (TCs) closest to the outlying center. Normalized data (Z-scores) were used for KCA input to lessen the effects of outlying data. The results of the final KCA output are discussed in the following Results chapter.

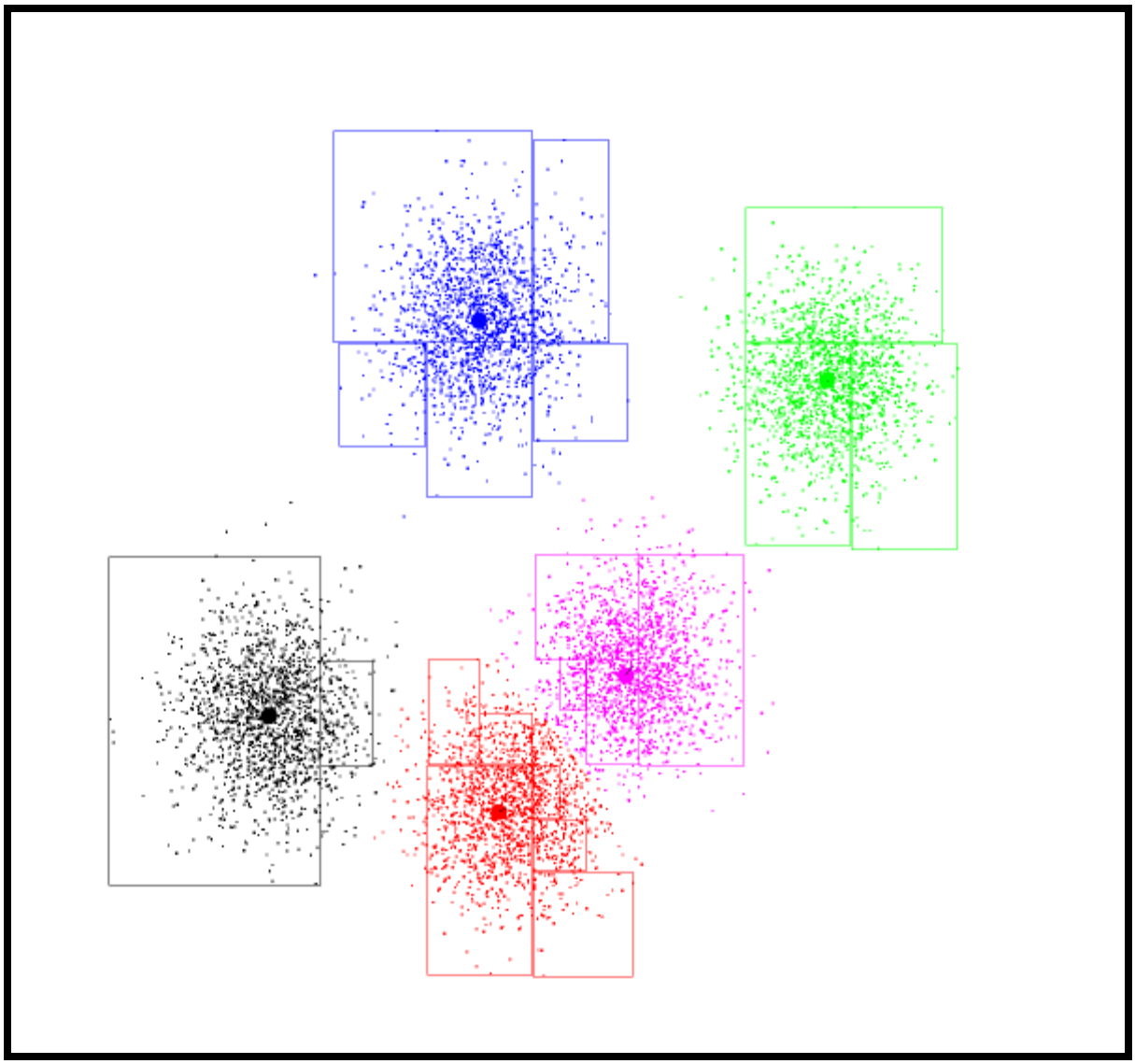

Figure 7: Example of K-Means clustering. Group membership is dependent upon distance of case values from the cluster center, which adjusts through multiple iterations until minimum distance between groups is achieved.

4. Results

The results of this thesis begin with a discussion of TC rain shield area (RSA) and traditional measures of TC size. The RSA discussion is followed by a summary of rain shield dissipation through twelve hours of landfall. Rain shield dissipation is examined by comparing the rate of dissipation by groups of TCs of similar size. This was accomplished by dividing the twenty-six TCs into three terciles according to their land-falling RSA. Observations of convective precipitation are examined in a similar manner to RSA. The results of the previously mentioned objectives are summarized by the proposed Tropical Cyclone Precipitation Hazard Scale (TCPH), the last section of the results. The TCPH was derived from the results of hierarchal and K-means cluster analysis.

a. Rain Shield Size and Precipitation Characteristics

The following sections discuss the TC rain shield in terms of size and precipitation intensity. Rain shield size is compared to traditional units of TC size and is observed through twelve hours after landfall. Traditional measurements of TC size typically cease within twelve hours after landfall as many TCs experience maximum winds that fall below tropical storm force. Precipitation intensity is described as either stratiform (light intensity) or convective (high intensity) and is partitioned by decibels of radar reflectivity. As in rain shield area, convective precipitation is described in terms of its areal extent within the rain shield.

1) Rain Shield Area

TC size varies considerably between storms. One of the largest tropical cyclones ever observed was Typhoon Tip that formed in the western Pacific in 1979. Conversely, one of the smallest ever observed was Cyclone Tracy that decimated Australia in 1974. Both TCs were extremely intense thus demonstrating one example of a well-documented, insignificant

relationship between storm size and maximum wind speed (Kaplan and DeMaria 1995). One objective of this thesis is to identify variability in storm size using two methods of assessment: rain shield area (RSA) and radius of the outermost closed isobar (ROCI). A depiction of RSA (bar graph) and ROCI (circles) for each TC in descending order of Vmax at landfall (t_0) is presented in Figure 8. Hurricane Ike (2008), a category 2 hurricane, had the largest ROCI at landfall and extended out 602 km; Hurricane Claudette (2001), a category 1 storm, had the shortest ROCI (167 km).

Hurricane Charley (2004), the only hurricane in this study to make landfall at category 4 strength (Vmax = 67 ms^{-1}) had a ROCI of 185 km. Previous research has established that no significant correlation exists between TC size (ROCI) and Vmax (Merril 1984), thus it was not unexpected that no relationship between RSA and Vmax was found here. This study found no significant relationship between the RSA and ROCI either. It is inferred from the findings of this study that RSA is a plausible unit of TC size, independent of the ROCI.

GIS composited images of the two largest TCs (by RSA at landfall), the two median, and the two smallest TCs are shown in Figure 9. Each storm in Figure 9 is presented at the same scale for relative comparison. The mean (median) RSA spanned 149,049 km^2 (143,149 km^2) at t_0. Hurricane Isidore (2002) had the largest rain shield (at t_0) spanning 333,765 km^2. Isidore reached category 2 status two days after its landfall in Cuba (20 September); however, by the time it made landfall in the United States (26 September) its maximum winds had weakened to 28 ms^{-1}, downgrading the TC to tropical storm (TS) status (NHC Archives). As a result, it was classified as a tropical storm for the purpose of this study, though it will be referred to as Hurricane Isidore as that is how it is listed in the NHC archives. Hurricane Danny (1997), a category 1 hurricane, had the smallest rain shield at t_0 (27,124 km^2). Despite its relatively weak winds and small size, it was a rather slow-moving hurricane and produced record rainfall in

coastal Alabama (Medlin et al. 2007) causing an estimated $100 million in damage throughout the lifetime of the storm (NHC Archives).

2) Rain Shield Dissipation

Boxplots of RSA are presented in Figure 10. There is little variability in the central measures of the dataset as there is less than a 5% difference between mean and median values in RSA at each time-step. A slight increase in median RSA is noticed between t_0 and t_{+6}, followed by a decrease from t_{+6} to t_{+12}. A Wilcoxon Rank Sum Test indicates that neither of these changes are statistically significant.

It is a generally accepted notion that the rate of maximum wind speed decay is larger than that of rain shield dissipation (Emanuel 2005). This section seeks to make direct comparisons of wind speed decay and rain shield dissipation through normalized variables, and then evaluate rain shield dissipation more thoroughly in the succeeding paragraphs. The normalization technique utilized is a simple Z-score (equation 1) analysis of RSA and TC maximum winds (as well as convective precipitation). Three observations were taken of each TC, totaling seventy-eight observations in all. Z-scores were calculated by computing the mean and standard deviation of all values of the three variables and then regrouped according to time respective to landfall (t_0, t_{+6}, and t_{+12}). Mean Z-score values at t_0, t_{+6}, and t_{+12} for RSA, CPA, and Vmax are plotted in Figure 11. Some broad generalizations can be derived from Figure 11: First, Vmax is accentuated at landfall. The Z-score values in Figure 11 are averaged over the entire dataset, therefore a Z-score of 0.77 for Vmax is representative of 42 ms^{-1} winds (a category 1 hurricane bordering on category 2 status) at landfall. Rain shield size, and more importantly, convective precipitation, decrease at such a rate that their Z-score values surpass that of Vmax between t_{+6} and t_{+12}. At t_{+6} only two TCs fell below tropical storm status, however seven had Vmax values

below damaging force (26 ms^{-1}) and fourteen were downgraded from hurricane status. At t_{+12} all but two TCs (Charley and Frances) had sub-hurricane-force winds. In all, 10% of the observations between t_0 to t_{+12} were of TCs that had Vmax values below tropical storm strength, 29% below damaging force, and 58% below hurricane force. It was attempted to show in Figure 11 a quantitative comparison of wind speed decay versus rain shield dissipation using a common metric; the risk associated with each hazard relative to one another is not implied in Figure 11.

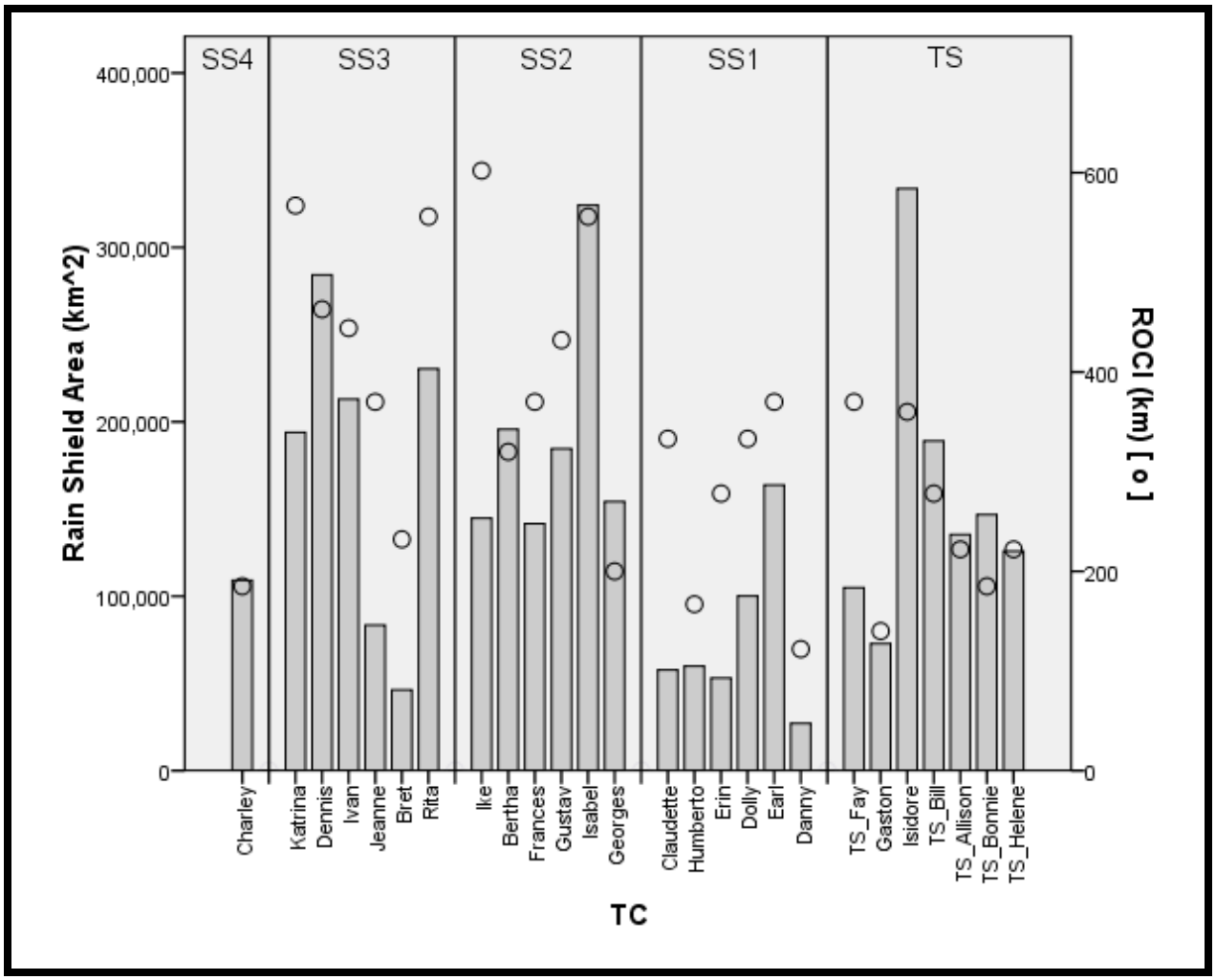

Figure 8: Categorical comparisons of rain shield area and radius of outer closed isobar, in decreasing order of maximum sustained wind speed.

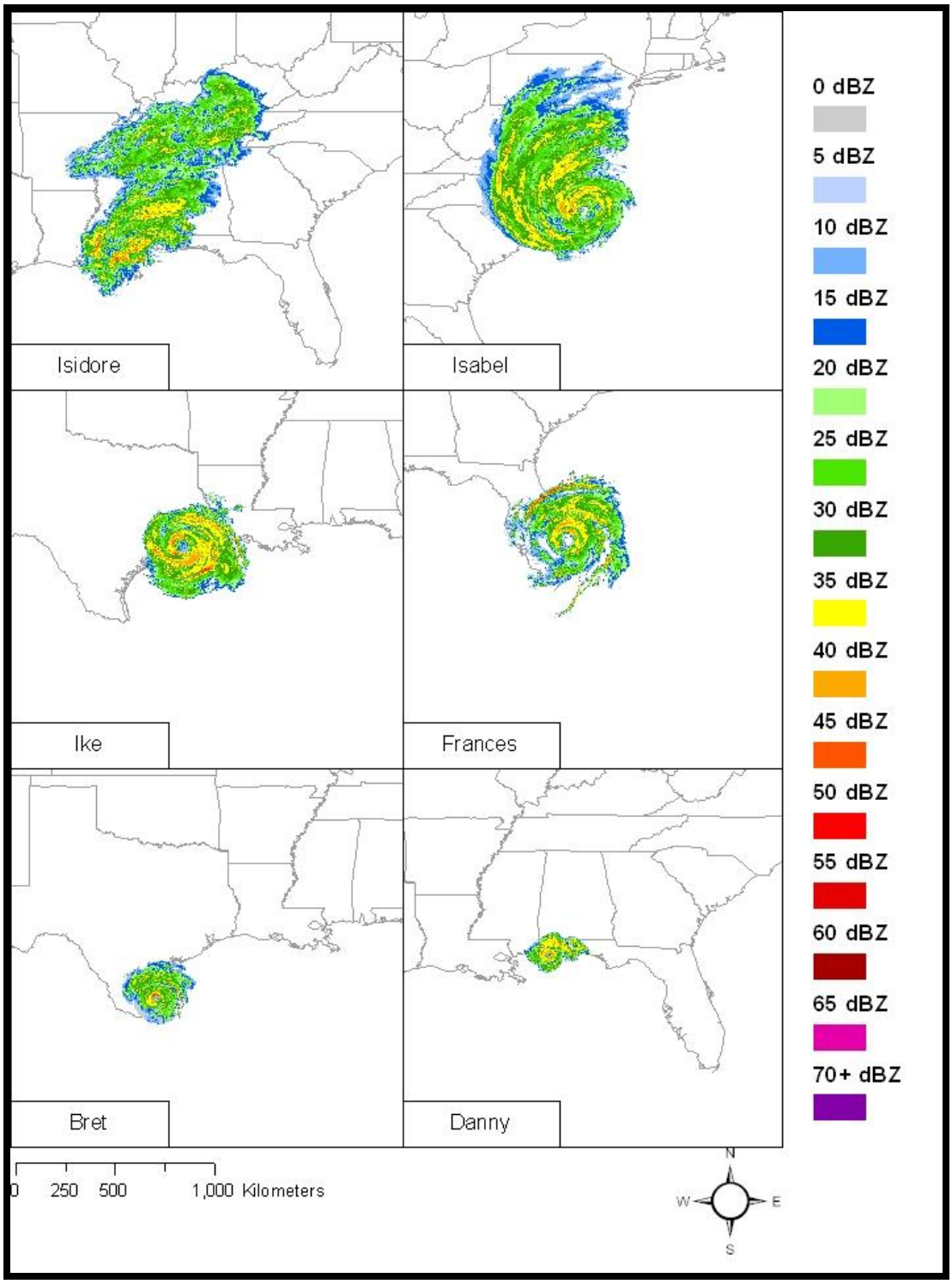

Figure 9: Same-scale comparisons of the two largest, two median, and two smallest TC rain shields of the twenty-six TCs in this thesis.

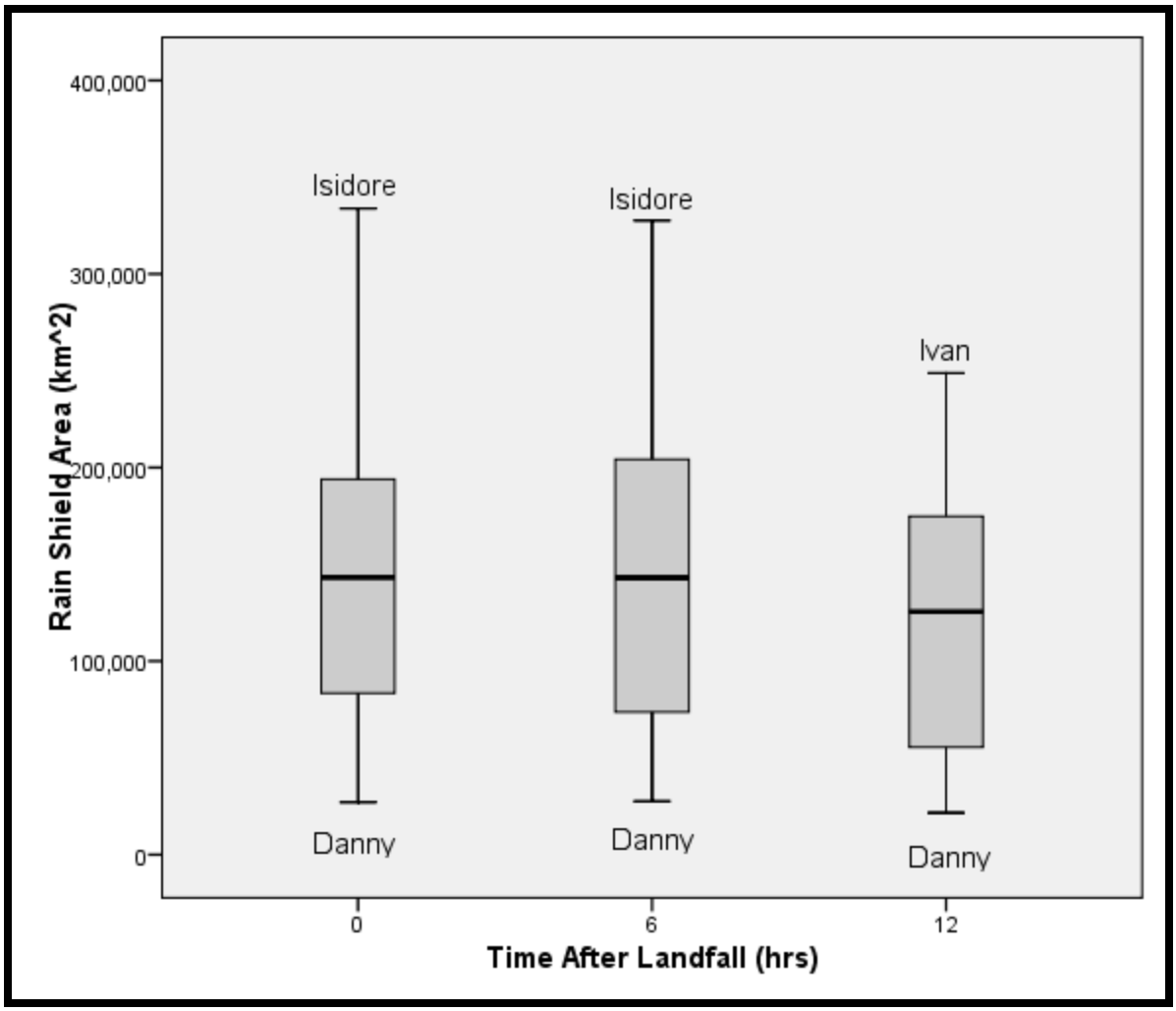

Figure 10: Boxplot diagrams of rain shield area of the twenty-six TCs at each time step in the study-frame of this thesis.

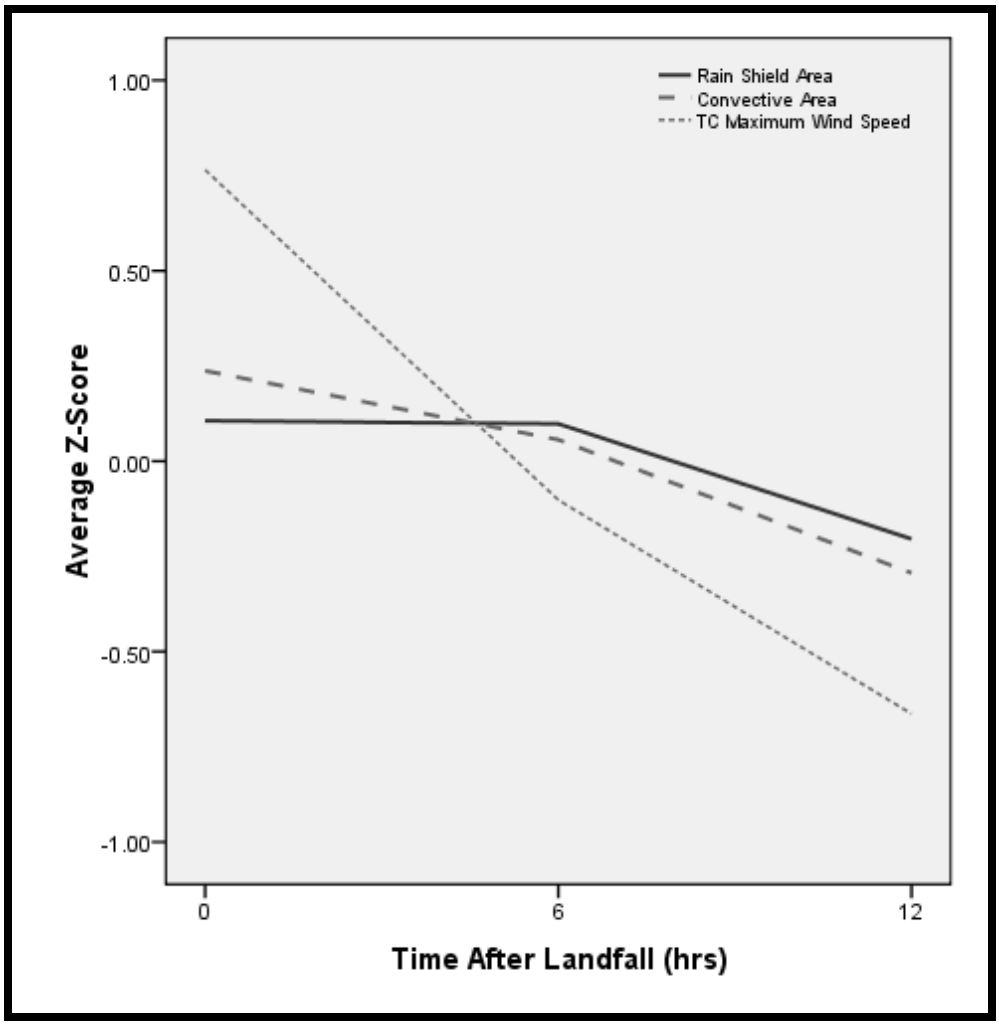

Figure 1: Z-score values of rain shield area, convective precipitation area, and maximum wind speeds at each time step.

3) Grouping TCs by Similar Size

TCs with similar Vmax decay at similar rates after landfall, making wind speed estimations reasonably predictable especially through twelve hours after landfall. This concept was applied to RSA dissipation of TCs with similarly sized rain shields. The twenty-six TCs were grouped into terciles according to their land-falling RSA. Box-plots of RSA for each tercile are depicted in Figure 12 at each of the three time-steps. There is generally good agreement between central measures for each tercile; median values of RSA for the largest tercile (T3) and median tercile (T2) vary less than 10% from mean values for each time-step while the smallest tercile (T1) exhibits more variability as medians vary by 12%, 28%, and 23% from mean values at t_0, t_{+6}, and t_{+12} respectively. Overlap between the range of RSAs is noticeable at t_{+6} and the inner quartile range (IQR, the difference between third quartile [Q_3] and the first quartile [Q_1]) overlaps between T2 and T3 at t_{+12}. Median RSA values for T3 show an increase between t_0 – t_{+6} while T2 and T1 median RSAs indicate a slight decrease. Mean RSA values for T3 show a decrease from t_0 – t_{+6} while mean RSAs for T2 and T1 indicate an increase. This partially explains the insignificant change in RSA determined by the Wilcoxon tests. Outliers were identified for cases that exceeded:

$$Q_3 \times 1.5\ \mathrm{IQR} \tag{3}$$

Hurricanes Isidore and Isabel were identified as outliers in T3 at t_{+6} as they were 1.4 and 1.7 standard deviations above the T3 mean respectively; Isidore and Isabel's RSAs were 2.1 and 1.9 standard deviations above the mean when compared to all twenty-six TCs at t_{+6}. Medians for each tercile were lower between t_{+6} and t_{+12}. Hurricanes Humberto and Jeanne were identified as outliers at t_{+12}, which is explained by the fact that both storms had expanding rain shields throughout the twelve hour period. Eight or nine TCs comprise each tercile, which is an insufficient sample size to conduct any meaningful statistical analyses between the size groups.

Fourteen of the twenty-six TCs were larger at t_{+6} than they were at t_0 and all expanding rain shields increased by 500 km^2 or more with nine of the fourteen increasing by 10,000 km^2 or more. Seven of the fourteen expanding TCs were in the first tercile, which accounts for the slight increase in mean area between $t_0 - t_{+6}$ in Figure 12. Hurricane Earl (1998) experienced the most RSA expansion by increasing by ~77,400 km^2 six hours after landfall. Hurricane Humberto (2007) doubled its rain area increasing from ~59,800 km^2 at t_0 to ~119,500 km^2 at t_{+6}. The top five expanding TCs from $t_0 - t_{+6}$ and from $t_{+6} - t_{+12}$ are listed in Table 3.

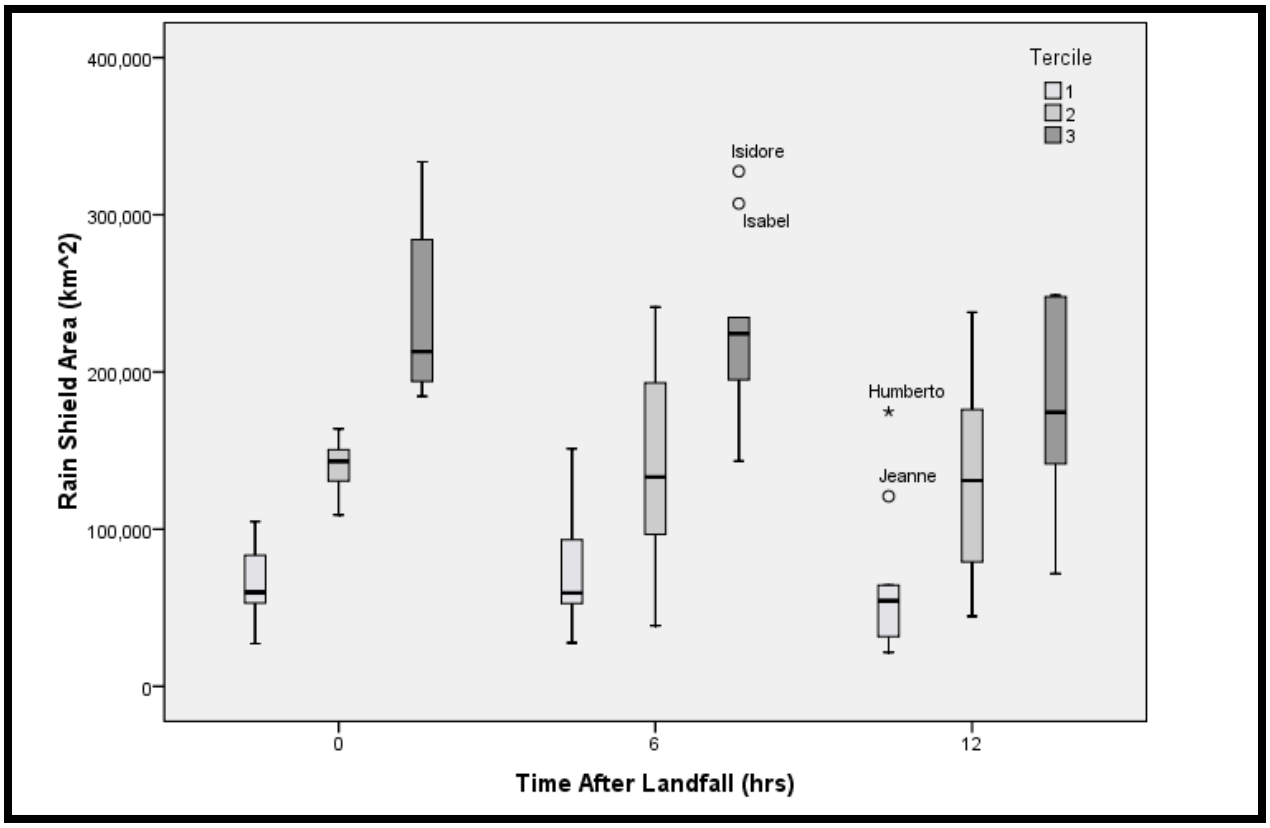

Figure 2: Boxplots of each tercile (based on rain shield area at landfall) at landfall plus six and twelve hours after landfall.

Table 3: Top expanding TCs.

TC Name	ΔRSA (km^2, $t_0 - t_{+6}$)
Earl	77,408
TS_Helene	63,291
Humberto	59,627
Frances	55,311
TS Fay	46,308
TC Name	**ΔRSA (km^2, $t_{+6} - t_{+12}$)**
Humberto	55,285
Bertha	43,534
Frances	41,119
TS_Allison	32,057
Jeanne	27,627

Table 4: P values for Wilcoxon rank sum tests.

Time Interval	RSA	CPA	Vmax
$t_0 - t_{+6}$	0.971	0.570	0.002
$t_{+6} - t_{+12}$	0.332	0.129	0.005
$t_{+0} - t_{+12}$	0.257	0.039	<0.001

Many meteorological variables present in mid-latitude climates are not found over tropical oceans, and the interaction of those variables with TC rain shields is an area of active research today (Atallah and Bosart 2003, Atallah et al. 2007, Garlineau et al. 2010, Matyas 2010). TCs have also been noticed to increase in size as a TC undergoes extratropical transition (Elsberry 2002), the results presented here show that TCs are almost equally likely (based on this thesis' relatively small sample size) to expand or dissipate immediately after landfall. Based on the small sample size presented here, it seems as though small TCs are most likely to expand after landfall before extratopical transition. The results of the previously mentioned Wilcoxon tests, which tested for significance in the change of the size of the precipitation areas (RSA and convective precipitation area) between two time steps (t_0 to t_{+6} and t_{+6} to t_{+12}) are summarized

in Table 4. The Wilcoxon test is similar to the paired t-test, which is a test in significance for the "before and after" change in a variable.

4) Convective Precipitation

It is important to determine the behavior of convective precipitation once a TC makes landfall as convective precipitation should pose a greater flood risk with its high rain rates. Landfall values of RSA and CPA for each TC are shown in Figure 13. It is apparent from Figure 13 that CPA is only weakly correlated to RSA. A total of seventy-eight observations were taken at landfall yielding an r^2 of 0.41 (Figure 14). Hurricane Rita (2005), a category 3 hurricane, had the largest total CPA (30,668 km^2) while Hurricane Bret (1999) had the smallest (2,350 km^2) at t_0. The CPA in Rita was larger than the entire rain shield of hurricane Danny. Interestingly, the TCs with the largest and smallest CPA were category 3 hurricanes. The top-5 TCs in terms of CPA included a tropical storm (TS Bonnie) and category 1 (Earl), 2 (Gustav), and 3 (Ivan and Rita) hurricanes. No correlation was found between Vmax and CPA ($r^2 < 0.05$).

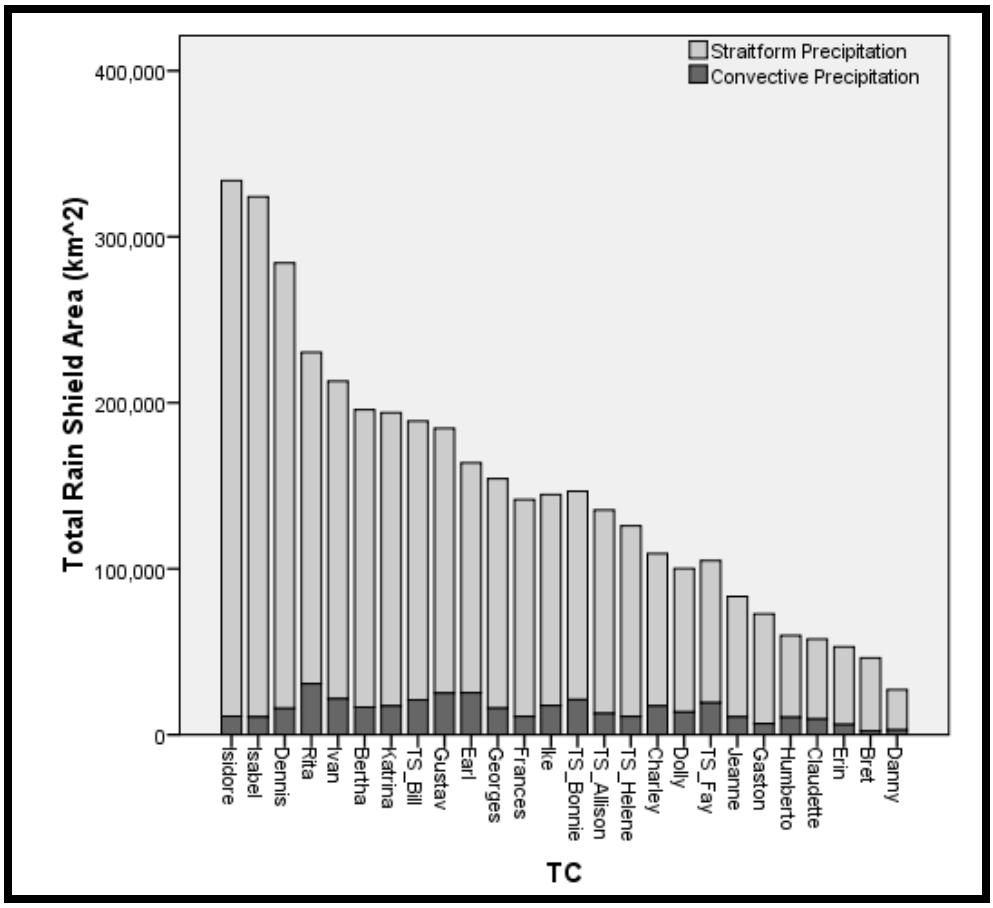

Figure 3: Area of convective precipitation vs. rain shield area (at landfall) of all twenty-six TCs.

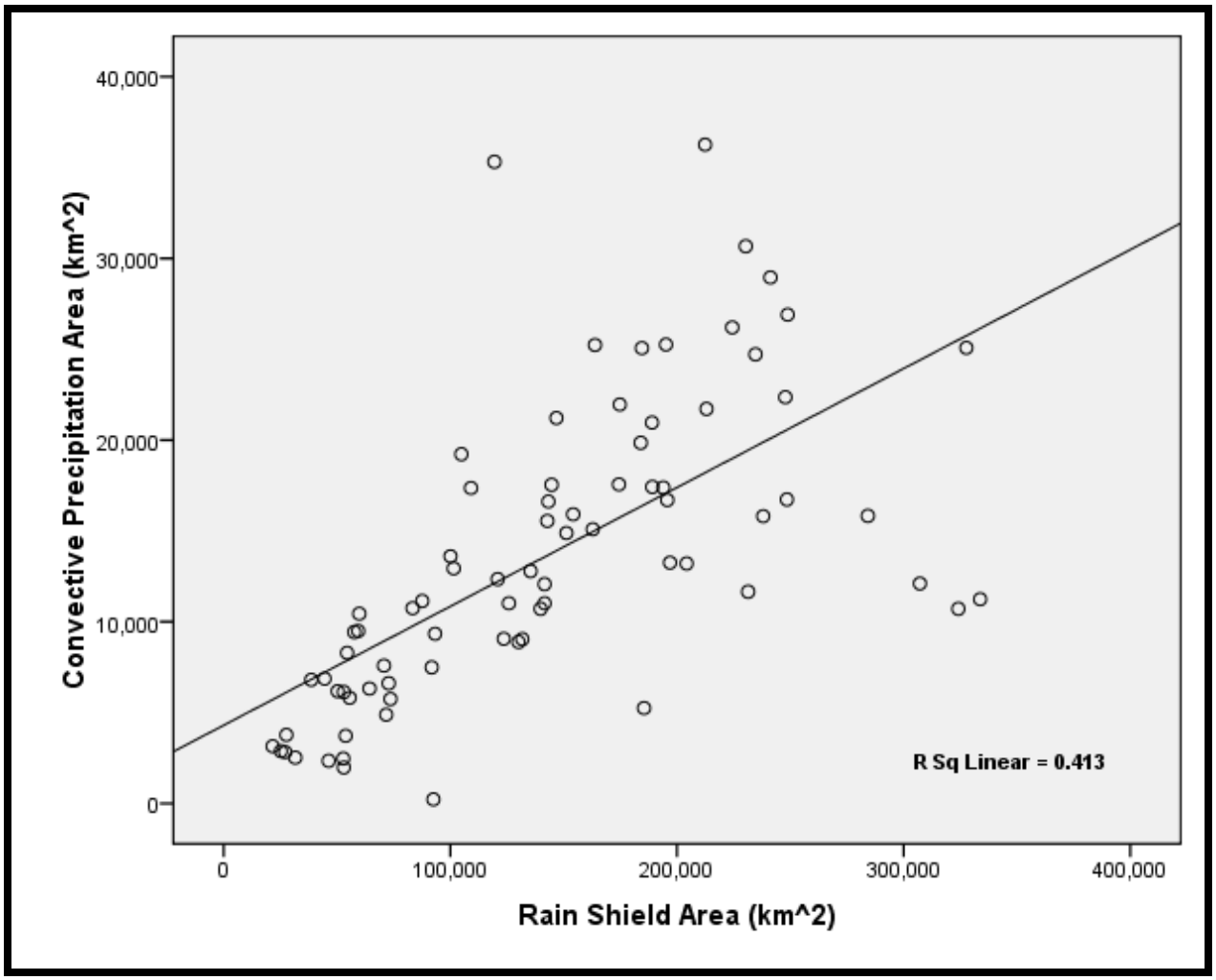

Figure 4: All observations (n = 78) of area of convective precipitation vs. rain shield area.

Boxplots of CPA at t_0, t_{+6}, and t_{+12} are shown in Figure 15. It is apparent between Figures 15 and 10 that CPA exhibits more variability than RSA. Hurricane Humberto (2007) was a small (T1) category 1 hurricane with small amount of +40 dBZ rainfall intensity at landfall that experienced rapid RSA expansion through t_{+6} and an even more rapid increase in CPA. It was mentioned in Section C that Humberto's RSA doubled between $t_0 - t_{+6}$; CPA in Humberto increased from ~10,400 km^2 to ~35,300 km^2 (+238%). This is quite a remarkable number as the areal expansion and percentage increase were both 3 standard deviations above the mean between t_0 and t_{+6}. Hurricanes Isidore and Katrina were the second and third most convectively expanding storms, increasing by ~13,800 km^2 and 8,800 km^2 respectively, compared to Humberto's expansion of ~24,900 km^2. Statistically, Isidore and Katrina's convective increases were 1.8 and 1.1 standard deviations above the mean (by area), which pales in comparison to Humberto's 3.2. At t_{+12} Hurricanes Earl and Ivan were identified as outliers (according to equation 3). Both TCs increased CPA from $t_0 - t_{+6}$ and $t_{+6} - t_{+12}$ by ~9,100 km^2 (Earl) and ~7,300 km^2 (Ivan). Hurricane Dolly (2008) had the next largest CPA increase at ~3,900 km^2.

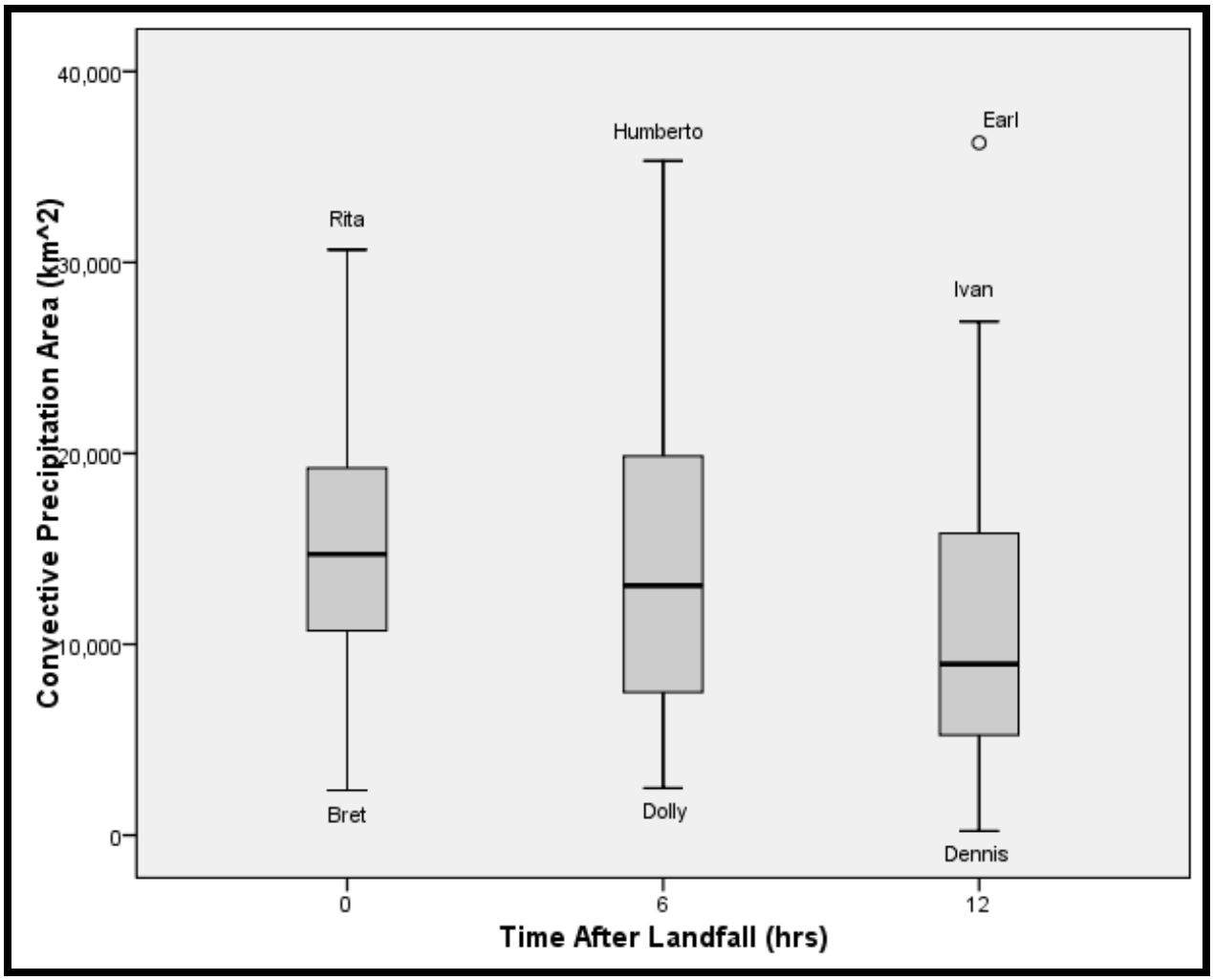

Figure 5: Boxplot diagrams of rain shield area of the twenty-six TCs at each time step in the study-frame of this thesis.

The next objective was to observe changes in RSA vs. changes in CPA from $t_0 – t_{+6}$ and from $t_{+6} – t_{+12}$. A graphical representation of changes in RSA (light bars) and CPA (dark bars) for TCs within each tercile from $t_0 – t_{+6}$ and $t_{+6} – t_{+12}$ are shown in Figure 16. Seven of the fourteen TCs with expanding rain shields from $t_0 – t_{+6}$ were in T1; Hurricanes Dolly and Gaston were the two TCs in T1 that dissipated within the first six hours after landfall. Twelve TCs increased in CPA from $t_0 – t_{+6}$, and ten of those twelve had increasing RSAs as well. Three TCs had CPAs that expanded by less than 1000 km^2. Isabel and Isidore were the two TCs that had dissipating RSAs and expanding CPAs. Interestingly, Isabel and Isidore were the two TCs that had atypically large

RSAs at t_{+6}. Also in Figure 16A three TCs had increasing RSAs with decreasing CPAs; twenty of the twenty-six TCs had rain shields that had common changes between RSA and CPA. Changes in RSA and CPA between $t_{+6} - t_{+12}$ are shown in Figure 16B. T3 TCs showed a rapid RSA dissipation as five decreased by 50,000 km^2 or more; Isabel, Dennis, and Katrina all dissipated by over 100,000 km^2. Relative to the mean dissipation, Isabel, Dennis, and Katrina decreased by 1.8, 2.1, and 2.3 standard deviations respectively. The corresponding decrease in CPA between the three was ~6,900 km^2 (-0.5 standard deviations), ~11,400 km^2 (-1.2), and ~21,300 km^2 (-2.7). Eight TCs increased in CPA between $t_{+6} - t_{+12}$, six of these increased in RSA as well. Hurricane Erin's RSA dissipated by ~18,000 km^2 and its CPA was computed to have only increased by 68 km^2, a rather ambiguous result. Of the nine TCs expanding in RSA during this time-step, six also increased in CPA. 79% of the observed changes in rain shields between $t_0 - t_{+6}$ and $t_{+6} - t_{+12}$ resulted in CPAs that expanded (dissipated) when RSAs expanded (dissipated); thus, it seems that when a TC's RSA expands after landfall, a coincident increase in CPA seems to be more likely than for the CPA to decrease.

Convection is not as enduring from t_{+6} to t_{+12} as rainfall intensity tends to weaken more rapidly within six to twelve hours according to Wilcoxon tests ($p = 0.129$). These results are generalized for all the TCs in this study as there was too much variability in the dataset to group convective areas. These results are based on our definition of the TC rain shield; no standard definition of the horizontal limits of TC rainfall are currently in use though other researchers have provided loosely based dimensions of the rain shield (Willoughby et al. 1984, Cecil et al. 2002).

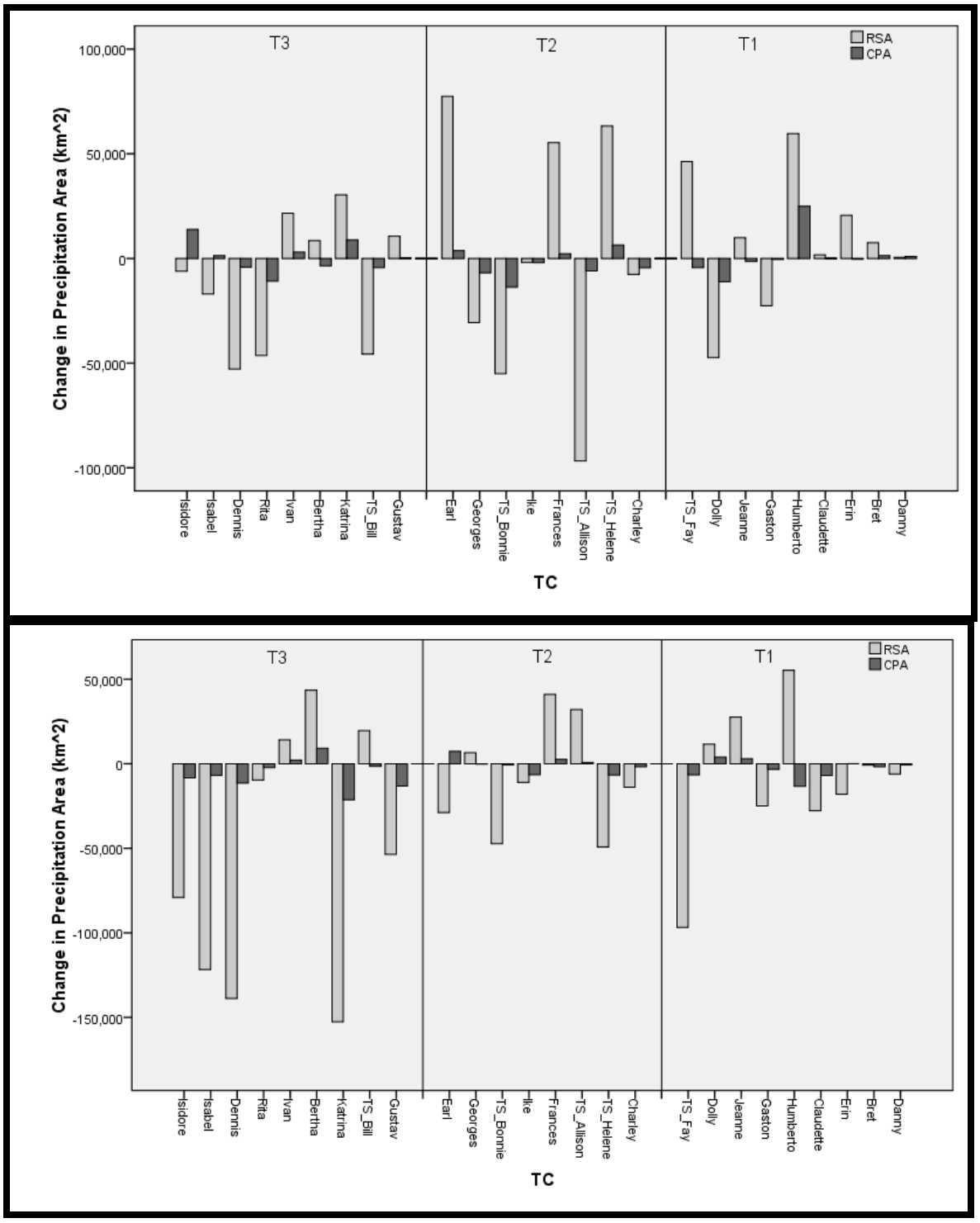

Figure 6: Graphical depictions of changes in rain shield area and convective precipitation area between $t_0 - t_{+6}$ and $t_{+6} - t_{+12}$.

The ratio of convective to stratiform precipitation was calculated in Jorgensen (1984) to be approximately 8.6% when averaged between Hurricanes Frederic and Allen. For the sake of comparison, convective ratios were computed in this study and were in relatively good comparison as the mean ratio for every TC at every time step was 11.8% with a standard deviation of 5.9%. Ratios ranged as high as 42.0% in Hurricane Humberto (at t_{+6}) and as low as below <0.00% in Hurricane Dennis (at t_{+12}).

b. Classification of TCs by Precipitation Variables

The Tropical Cyclone Precipitation Hazard Scale was derived from the results discussed above. The following sections describe the results of cluster analysis used to determine group membership of each TC. A discussion of the precipitation characteristics each group also follows.

1) The Tropical Cyclone Precipitation Hazard Scale (TCPH)

The above analysis led to the proposition of the Tropical Cyclone Precipitation Hazard Scale (TCPH). The term velocity refers to the average forward speed of the storm as TC wind speeds are neglected in this classification scheme. The scale emphasizes the aforementioned variables to categorize the risk associated with TC-induced flooding. Three precipitation variables (rain shield area, change in rain shield area, and convective precipitation area) were ranked on a 1–4 scale (P^{1-4}) and velocity was categorized as either fast (v^{+}), average (), or slow (v^{-}). A depiction of these designations is provided in Figure 17. All TCs have a precipitation ranking while velocity designations are given only to TCs classified as either fast or slow. Fast or slow designations were generally assigned when the group mean Z-score was greater or less than 1 standard deviation. There were instances where fast- or slow-moving TCs were assigned to groups not

designated as v^+ or v^-. Precipitation variables were ranked subjectively and a rationalization of these rankings are briefly presented below.

K means Cluster analysis revealed six groups. Indubitably, more TCs will make landfall in upcoming years and this scale is amendable to accommodate changes that may be necessary as the current sample size is rather limited. Group membership for each cluster is listed in Table 5; also shown in Table 5 is each TCs Z-score values for each of the four variables used in analysis. A description of each group follows.

Rain Shield Description	P Symbol	Velocity	v Symbol
Small	P^1	Fast	v^+
Expanding	P^2	Slow	v^-
Large	P^3		
Convective	P^4		

Figure 7: Description of the symbology of the Tropical Cyclone Precipitation Hazard Scale.

Table 5: Group membership of each cluster in the proposed TCPH scale.

TC	RSA	ΔRSA	CPA	AvgFwdSpd	SS	TCPH
Claudette	-1.13	-0.05	-0.74	-0.11	1	$\mathbf{P^1}$
Erin	-1.19	0.39	-1.21	0.44	1	
Jeanne	-0.80	0.93	-0.55	-0.35	3	
TS_Allison	-0.15	-0.64	-0.26	-0.63	TS	
TS_Helene	-0.27	0.56	-0.51	0.70	TS	
Mean	**-0.71**	**0.24**	**-0.66**	**0.01**		
Bret	-1.27	0.45	-1.76	-1.24	3	$\mathbf{P^1v^-}$
Danny	-1.51	0.27	-1.69	-2.00	1	
Dolly	-0.59	-0.20	-0.14	-1.15	1	
Gaston	-0.94	-0.38	-1.15	-0.89	1	
Mean	**-1.08**	**0.03**	**-1.18**	**-1.32**		
Bertha	0.61	1.15	0.30	0.76	2	$\mathbf{P^2}$
Frances	-0.07	1.83	-0.51	-0.96	2	
Georges	0.09	-0.02	0.19	-1.42	2	
Humberto	-1.10	2.11	-0.60	-0.49	1	
Mean	**-0.12**	**1.27**	**-0.15**	**-0.53**		
Dennis	1.06	-1.78	-0.42	0.56	3	$\mathbf{P^3}$
Isabel	2.23	-1.78	-0.56	1.26	2	
Isidore	2.35	-0.96	-0.48	0.73	TS	
Mean	**1.88**	**-1.51**	**-0.49**	**0.85**		
Earl	0.21	1.10	1.53	0.79	1	$\mathbf{P^4}$
Gustav	0.47	-0.31	1.50	0.18	2	
Ike	-0.03	0.15	0.42	0.14	2	
Ivan	0.83	0.90	1.02	0.11	3	
Rita	1.05	-0.51	2.30	-0.20	3	
TS_Bill	0.53	-0.05	0.91	0.25	TS	
TS_Fay	-0.53	-0.42	0.66	-0.90	TS	
Mean	**0.36**	**0.12**	**1.19**	**0.05**		
Charley	-0.48	0.02	0.40	1.57	4	$\mathbf{P^4v^+}$
Katrina	0.59	-1.53	0.40	0.49	3	
TS_Bonnie	0.00	-1.22	0.95	2.36	TS	
Mean	**0.04**	**-0.91**	**0.58**	**1.47**		

i) Small TCs (P^1)

P^1 TCs are characterized best by relatively small rain shields with small convective areas and thus are given the lowest P ranking (P^1). All five TCs in this cluster had RSA and CPA Z-scores < 0.00 (at landfall). Hurricane Jeanne was the most destructive TC of this group (NHC archives), which is likely the result of its category-3 winds. Jeanne had the largest CPA of the TCs in this cluster. Reanalysis images of the five P^1 TCs (Figure 18) show rain rate (mm/day) contours averaged over the day of landfall (and the subsequent day if the TC made landfall during 1201 – 2359 UTC). Notice that Hurricane Jeanne had the largest rain rates of any P^1 TC (Figure 18). From a flood hazard standpoint, the TCs in this cluster would be least likely to cause catastrophic flooding over a large spatial distance. Tropical Storm Allison (2001) seems to be an anomaly in this category; as much as 890 mm of precipitation were measured in the Houston metropolitan area causing damage estimates nearing as much as $5 billion (NHC archives) over the lifetime of the storm. Allison was a slower-than-average storm (translational velocity of 4 ms^{-1}) that passed directly over Greater Houston. Despite Allison's below average CPA (Z-score = -0.26), the majority of convective precipitation was oriented north of the storm track directly over the densely populated Texas Gulf Coast. Figure 19A shows a population density map of the Texas Gulf Coast with three storm center points of Allison (at t_0, t_{+6}, and t_{+12}) as it tracked over Houston. Rainfall intensity is shown in Figure 19B; the northward-oriented convective cell is clearly visible as it is centered over densely populated Greater Houston. Convection in Allison's core increased from $t_0 - t_{+6}$, and this increase in CPA combined with the storms slow translational velocity resulted in prolific flooding and 23 recorded fatalities in Texas. Radar estimated rainfall (Figure 19C) shows the highest accumulated rainfall occurred over Greater Houston. A range from 102 to 203 mm fell in the three hours after landfall over the most populous areas of Houston. Precipitation

distribution is not categorized in the TCPH scale though Allison, which never attained hurricane status, serves as an illustration that slow moving storms with heavy precipitation concentrated over densely populated locations have the potential to cause remarkable damage and produce fatalities.

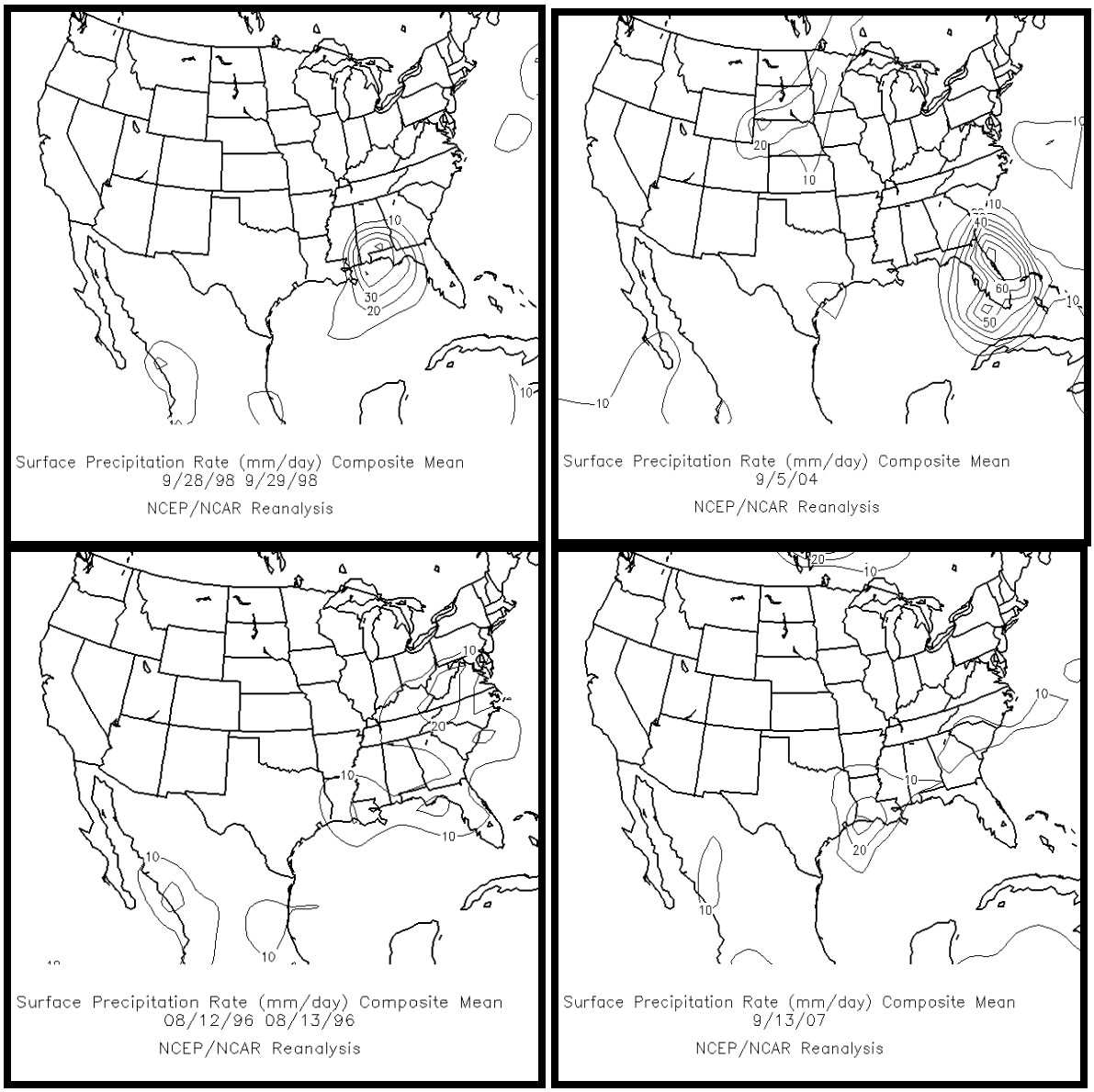

Figure 8: Daily mean composite rain rate reanalysis maps of P[1] TCs reproduced from the Earth Systems Research Laboratory website (http://esrl.noaa.gov/psd/data/composites/day/).

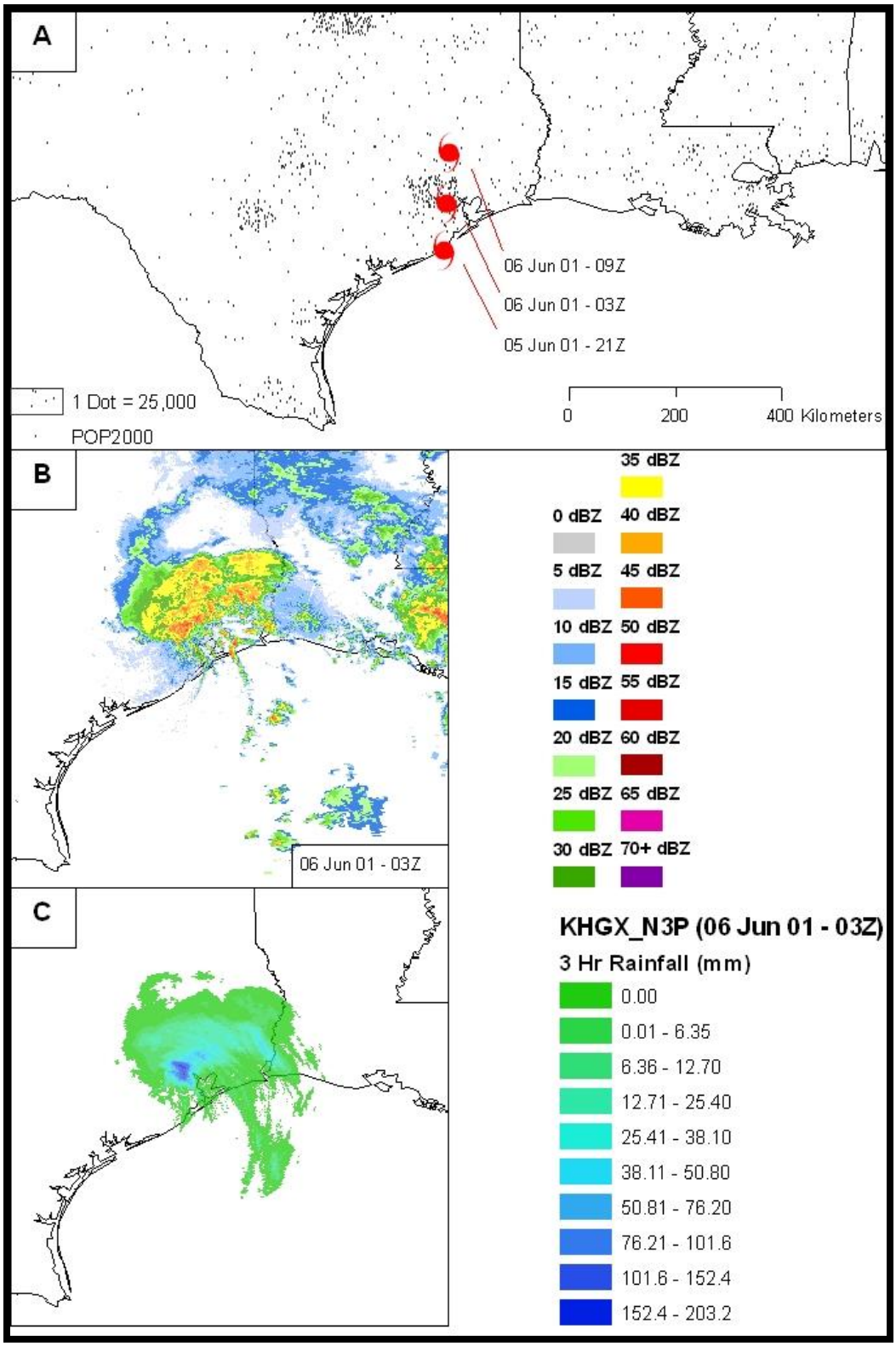

Figure 9: GIS images of Tropical Storm Allison's (2001) track (A), rainfall intensity (B), and 3 hour accumulated rainfall (C).

ii) Slow-moving, small TCs (P^1v^-)

P^1v^- TCs were similar to P^1 TCs in that they had small rain shields with little convection (Z-scores for RSA and CPA for all TCs in this cluster were < 0.00) however P^1v^- storms had slow average forward velocities and thus, were given the v^- addendum. Three of the four P^1v^- TCs had average forward velocity Z-Scores < -1.00 (2.1 ms^{-1}). Hurricane Gaston was the fastest TC of P^1v^- storms with an average forward velocity of 3.7 ms^{-1}, which was slower than the slowest P^1 TC (Tropical Storm Allison, 4.4 ms^{-1}). Mean forward velocity in this cluster was 2.5 ms^{-1}, compare to the twenty-six TC average of 6 ms^{-1}; Hurricane Danny was nearly stagnant with an average forward velocity of only 0.6 ms^{-1}, this enabled record rainfall amounts in coastal Alabama (Medlin et al. 2007), which caused an estimated $100 million in damages through the lifetime of the storm (NHC archives). Hurricane Bret was a category 3 hurricane that made landfall in sparsely populated southern Texas and yielded half the insured losses of Danny, a category 1 storm.

iii) TCs with expanding rain shields between $t_0 - t_{+12}$ (P^2)

P^2 TCs are best categorized by TCs with expanding rain shields (based on the author's definition of the rain shield) between t_0 and t_{+12}. Growing TCs had a larger rain shield area at t_{+12} than at landfall, however this did not necessarily mean that rain shield growth was observed from t_0 to t_{+6} and t_{+6} to t_{+12}. It is possible for growing TCs to have a rather large growth in the TC rain shield between t_0 and t_{+6} and have a less rapid decay between t_{+6} and t_{+12}, though this was not the case for any of the storms in this study.

RSA was inconsistent in this category and had the highest variance between all the clusters, however RSAs for P^2 TCs generally were larger than P^1 TCs and smaller than P^3 TCs. No P^2 TC had an RSA greater than a P^3 TC (at landfall), though Hurricane Humberto (P^2) had

an RSA of only ~59,800 km^2 (RSA Z-score = -1.10) yet it expanded more than any TC in this study. Humberto nearly doubled in size between t_0 and t_{+6}, outpaced by only Hurricane Earl and Tropical Storm Helene. Humberto grew in relative size more than any other TC from t_0 – t_{+6} (~100%). The next highest relative increase was TS Helene, which increased by ~50% of its landfall value). Humberto increased by another ~55,300 km^2 from t_{+6} – t_{+12}, a total increase of ~114,900 km^2 over twelve hours, more than any other storm in the study.

Three other TCs were classified as P^2 storms: Hurricanes Bertha, Georges, and Frances. Behind Humberto, Bertha and Frances gained more RSA through twelve hours than any other TC. Hurricane Georges actually lost RSA between t_0 – t_{+12}, this loss was relatively small (Z-score for ΔRSA = -0.02) and based on the Z-scores for Georges' other variables, it seems the K-means analysis found it most fitting in this cluster. Bertha, Frances, and Georges were category 2 hurricanes as all three TCs had 46 ms^{-1} maximum winds at landfall.

iv) Large TCs (P^3)

P^3 TCs have large rain shields that were not predominately convective. Hurricanes Dennis, Isabel, and Isidore (a tropical storm at landfall) were designated as P^3 storms. Only three TCs made up this group and characteristics of each TC in each of the four variables were fairly uniform. P^3 TCs were the only TCs with uniform characteristics in terms of having Z-scores ± 0.00. The three TCs in this cluster were all large tropical cyclones with little convection that rapidly decayed after making landfall. Surprisingly, P^3 were faster moving than average as all three TCs had Z-scores > 0.5 and a mean translational velocity of ~9 ms^{-1}. This group was not designated as fast-moving owing to two of the three TCs having Z-scores for average forward velocity < 1.00 and the group mean equal to 0.85; the designation to classify this group as having average speed was made subjectively, and if two of the three

TCs and the group mean had Z-scores above 1.00, the group would have been designated as fast-moving. Hurricane Isabel covered over 324,000 km^2 at landfall and lost 43% of its rain shield through twelve hours. Despite having the second most-rapidly decaying rain shield (from $t_0 - t_{+12}$), Isabel covered over 185,000 km^2 at t_{+12}, which was larger than $^2/_3$67% of the landfall values for the other TCs in this study. Hurricane Dennis, the third largest TC (at t_0) and most-rapidly decaying TC of this thesis, dissipated nearly 192,000 km^2 of its rain shield (67% of its landfall amount) from t_0 to t_{12}. Convective precipitation showed some relationship with storm size (Figure 14), however, these three TCs had below average amounts of convective precipitation despite their large rain shields.

v) TCs with high amounts of convective precipitation

P^4 TCs have the largest CPAs, which, in turn, bring the highest rain rates and theoretically would have the highest inherent flood risk. P^4 TCs comprised the largest group of this thesis with seven members: Hurricanes Earl, Gustav, Ike, Ivan, and Rita, and tropical storms Bill and Fay. CPA is an indirect measure of storm size as widespread areas of convective precipitation will be embedded into a relatively large rain shield. CPA shares a modest correlation to RSA (Figure 14). Z-Score values for CPA ranged from 0.42 (Ike) to 2.30 (Rita) with four of the seven TCs having Z-Scores >1.00. The average convective area for all twenty-six TCs covered 14,759 km^2, Hurricane Ike's CPA spanned 17,538 km^2 while Rita's CPA totaled 30,668 km^2.

Reanalysis images of precipitation rate averaged over the day of landfall show that P^4 TCs have considerably higher rain rates compared to other groups in this classification scheme (Figure 21). Of particular note are Hurricanes Ivan and Rita, both of which had rain rates exceeding 90 mm/ day, more than any other of the TCs in this study.

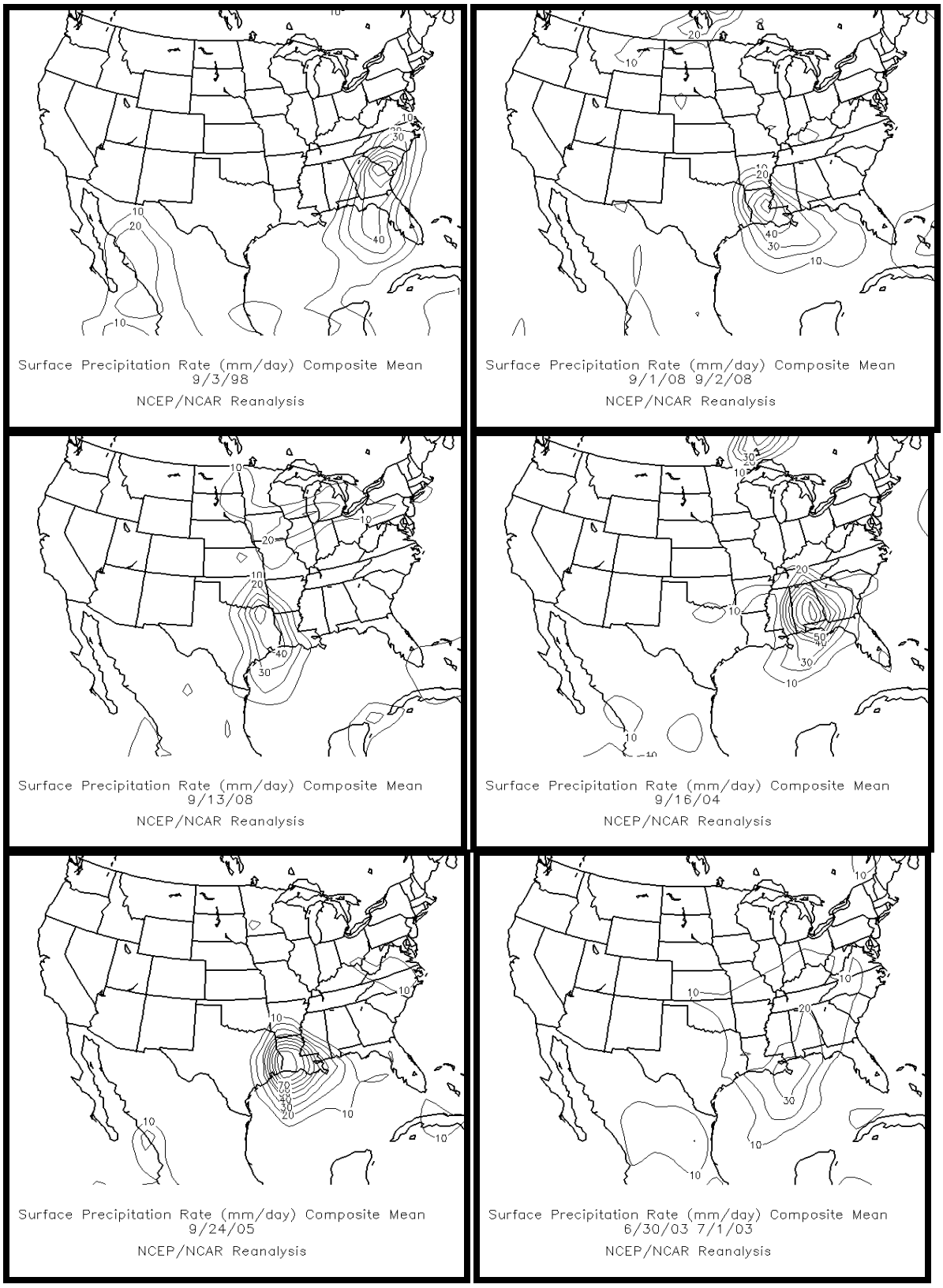

Figure 10: Daily mean composite rain rate reanalysis maps of P^4 TCs reproduced from the Earth Systems Research Laboratory website (http://esrl.noaa.gov/psd/data/composites/day/, TS Fay not shown).

vi) Fast moving convective TCs (P^4v^+)

P^4v^+ TCs are, as a group, fast-moving TCs with moderate amounts of convection. This is perhaps the most ambiguous cluster of the scheme. The foremost feature of this group is the fast forward velocity of the three TCs. When assigning a precipitation characteristic, CPA was the variable with the least amount of variance and was the only precipitation variable where all three TCs shared the same Z-score sign (± 0.00) and thus, the precipitation characteristic was designated as convective (P^4). This (along with P^3) is the smallest group of the TCPH Scale. It is comprised of Hurricanes Charley and Katrina and Tropical Storm Bonnie. Charley was the only TC to make landfall as a category 4 hurricane in this study, however the fast translational velocity of this storm (12 ms^{-1}) likely mitigated the effects of prolonged exposure to convective precipitation that could have possibly inflicted greater flooding. The NHC's Hurricane Preparedness website (http://www.nhc.noaa.gov/HAW2/english/intro.shtml) shows the extent of hurricane winds from a fast moving hurricane (Figure 21A) and slow moving hurricane (Figure 21B). Tropical Storm Bonnie had the largest convective area (at landfall) of P^4v^+ TCs with its CPA covering ~21,200 km^2, comparing to ~17,400 km^2 and 10,700 km^2 of Hurricanes Charley and Katrina respectively. Bonnie also had the largest CPA of all tropical storms in the dataset. Bonnie's average forward speed of approximately 13 ms^{-1} made it the fastest moving of the twenty-six TCs, possessing a Z-Score of 2.36, the highest Z-score of any TC for any variable in the study and the only TC with a Z-score above 2.00 for average forward speed. Reanalysis images of precipitation rates (mm/ day) of the P^4v^+ TCs are shown in Figure 22; the fast forward motion of the TCs brings precipitation over a widespread area where it is noticeable that TC precipitation shows an elongation along the TC track of the fast moving P^4v^+ TCs. Notice in Figure 22 the large rain rates centered over southeast Louisiana coast; Katrina happened to be 2 ms^{-1} slower at t_0 than it was at t_{+6} and t_{+12}.

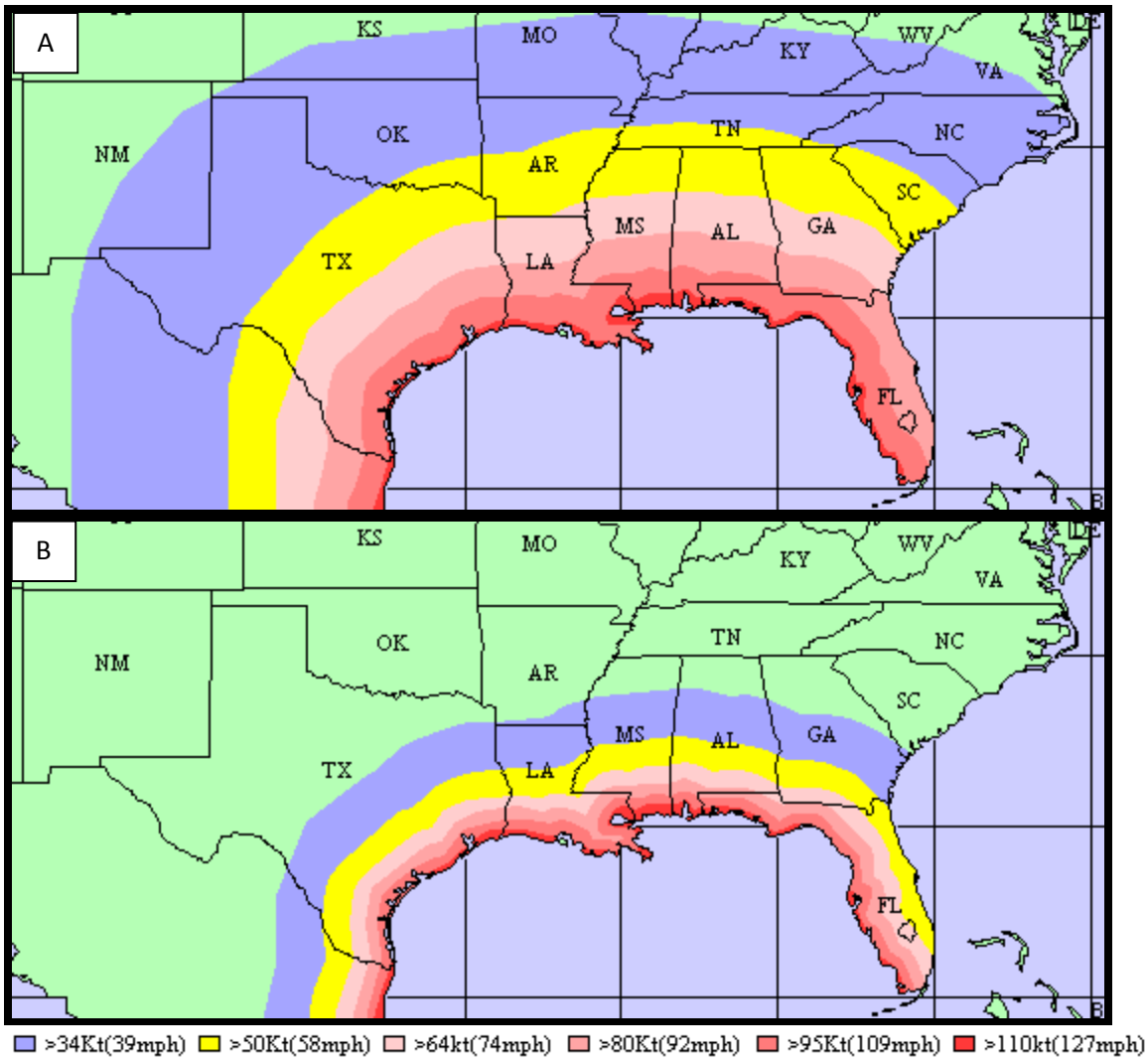

Figure 11: Wind swaths of a Gulf Coast landfalling Saffir-Simpson category 4 hurricane for a fast moving (A, 25 mph) and slow moving (B, 9 mph) storm. Images obtained online from the National Hurricane Center's Hurricane Preparedness website.

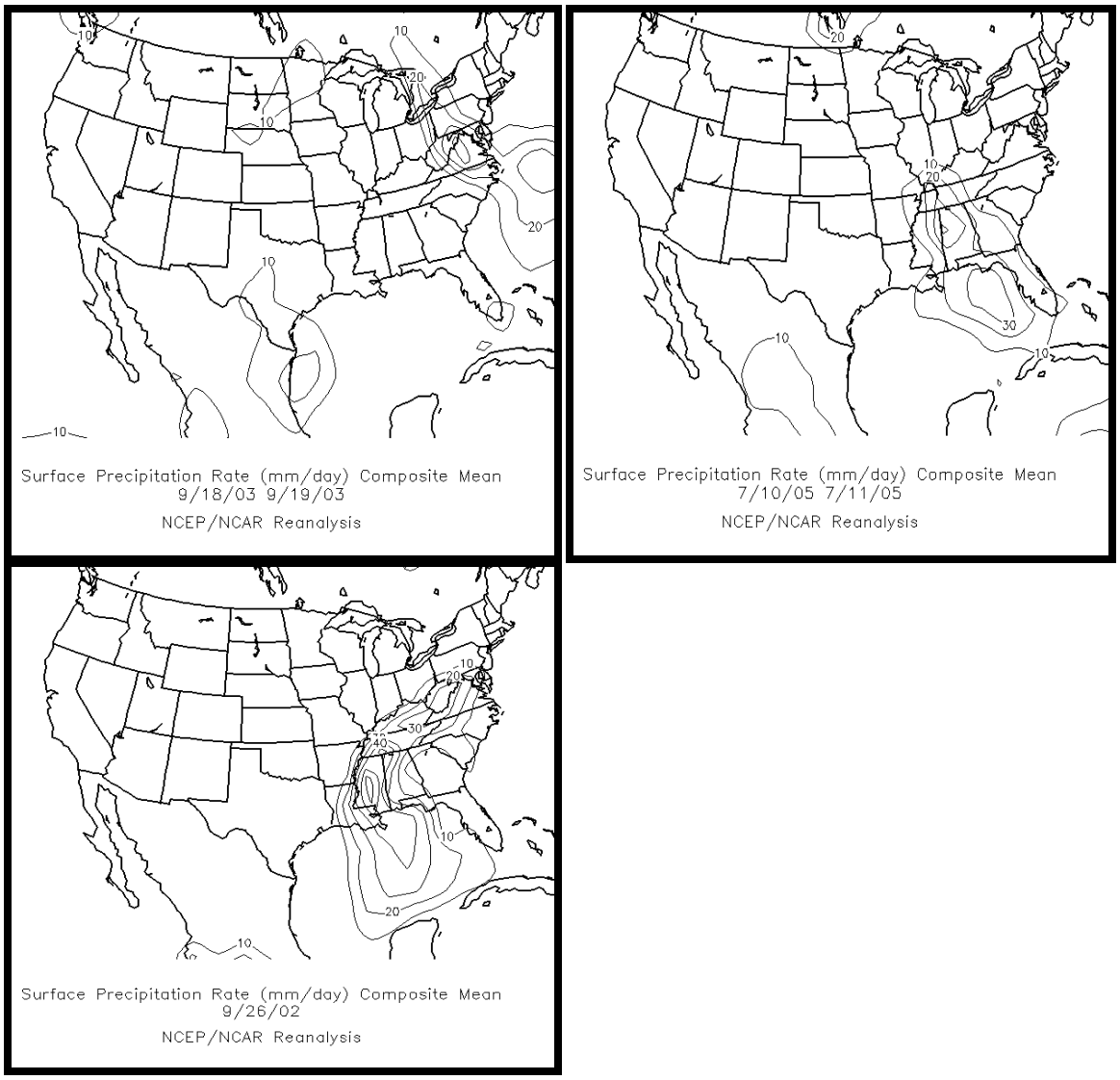

Figure 12: Daily mean composite rain rate reanalysis maps of P^4v^+ TCs reproduced from the Earth Systems Research Laboratory website (http://esrl.noaa.gov/psd/data/composites/day/).

Hurricane Katrina, arguably the greatest natural disaster in the United States in decades, made landfall in Buras, Louisiana on 29 Aug 2005 (1110Z), 90 km (56 miles) from New Orleans as a category 3 hurricane that was relatively large, convective, and fast, though it was not above one SD in any of these categories. A characteristic not accounted for in this scheme but no doubt contributing to the catastrophe of Katrina was the distribution of convective precipitation that was situated primarily to the north of the storm track as Katrina tracked nearly due north as it passed just east of New Orleans. Another contributing factor was its increase in RSA and CPA through six hours of landfall (rain shield dissipation was evaluated by differences in RSA between t_0 and t_{+12}) which is not accounted for in this classification scheme. This situation is similar to that of TS Allison in 2001. Similar to Figure 19, Figure 23A shows the track of Katrina over the Louisiana and Mississippi Gulf Coast. Also similar to Alison, intense convective precipitation was centered over the densely populated area surrounding New Orleans (Figure 23B). Three-hour, radar-estimated rainfall from Figure 23C shows the most rainfall accumulated near New Orleans. RSA (CPA) in Katrina increased from ~194,000 km^2 (~17,400 km^2) at t_0 to ~224,400 km^2 (~26,200 km^2) at t_{+6}, before rapidly dissipating to 71,700 km^2 (~4,900 km^2) at t_{+12}. Katrina's six-hour change in RSA between $t_{+6} - t_{+12}$ was the largest dissipation of all twenty-six TCs while its decrease in CPA was second only to Hurricane Dennis. This rapid dissipation took place well after it passed over New Orleans. Most of the flood damage from Katrina is attributed to the breakage of the city's levee systems (NHC archives) and not directly from precipitation-induced flooding. Katrina's measured rainfall (Figure 22) was the highest of the three p^4v^+ TCs and is similar to the primarily convective TCs discussed in the previous section. The below sea-level elevation of New Orleans (-2.4 m Mean Sea Level, http://egsc.usgs.gov) was undoubtedly another contributing factor to the Katrina disaster, and would be classified as a high risk location according to Baker (1991). It is unlikely that a single classification system can

assess Hurricane Katrina among other landfalling TCs as the disaster was a "perfect storm" in the sense that several meteorological, topographical, logistical, and socio-economic factors came to near perfect alignment for a catastrophe. Though true estimates of damage and loss of life may never be known, Hurricane Katrina is responsible for approximately $81 billion in damages and over 1,800 fatalities. Topography is unquestionably correlated to damage statistics from landfalling TCs. Katrina also shows that precipitation distribution is an essential component to the destructive potential of a TC. Summary statistics of the damage and socio-economic effects from Katrina can be found in Gabe et al. (2005), among various other sources.

2) Comparison of Insured Losses

Damage estimates and loss of life statistics were discussed on a case-by-case basis in this section. No direct comparisons were made between TCPH categories (nor were comparisons made with damage between TCPH and SS categories) as these numbers are, in addition to meteorological factors, dependent upon non-meteorological variables such as population density and vulnerability to the local infrastructure (Powell and Reinhold 2007). A comparison of mean total insured losses within each TCPH category is presented in Figure 24, proportioned by each TC in each cluster. This figure is a simplified estimation of damage potential for each TCPH category as it assesses insured losses only. Total damage estimation is generally computed by doubling insured losses (NHC archives). Also, total losses are computed throughout the lifetime of the storm and include damage from winds and flooding.

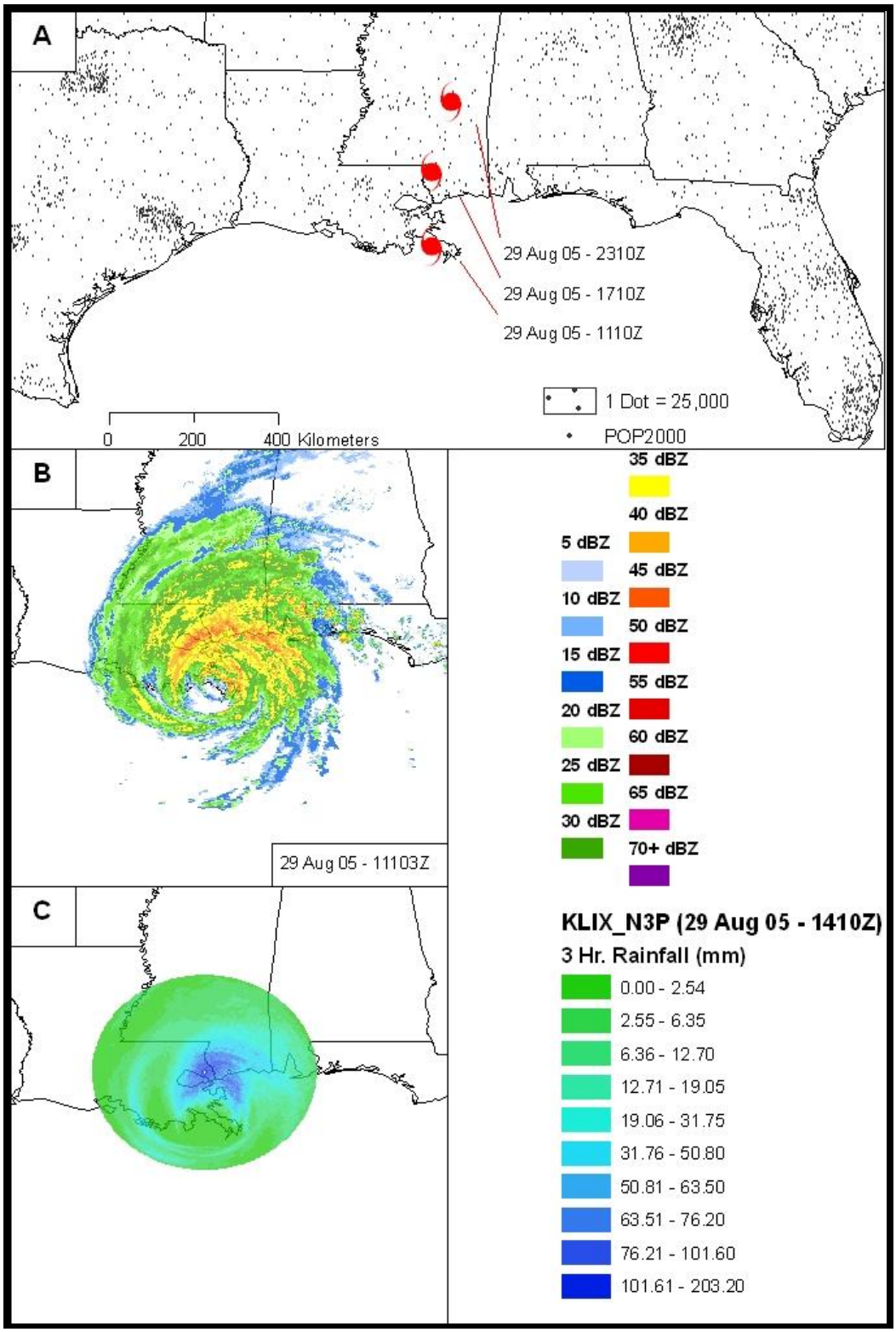

Figure 13: GIS images of Hurricane Katrina's (2005) track (A), rainfall intensity (B), and 3 hour accumulated rainfall (C).

Nonetheless, Figure 24 serves as a reasonable estimate of damage potential as the P^1 TCs generally inflicted the least amount of damage (though Tropical Storm Allison and Hurricane Jeanne both caused damages totaling over $1 billion) and P^4 TCs were the most damaging on average. It was hypothesized that slow moving TCs (v^-) would be potentially more damaging than fast moving TCs though the P^1 TCs as a group inflicted more damage than P^1v^- TCs. TC tracks reveal that the P^1 TCs traversed locales that were more densely populated than the tracks taken by the four P^1v^- TCs. Of the seven P^4 TCs, four were +$1 billion disasters (Hurricanes Gustav, Ike, Ivan, and Rita). Hurricane Ike, a category 2 hurricane, totaled over $12 billion in losses. Ike made landfall in the Greater Houston area 73 km (46 miles) from where TS Allison made landfall with a Vmax of 49 ms^{-1} (110 mph), compared to the 23 ms^{-1} (51 mph) of Allison's maximum winds. The higher maximum winds undoubtedly contributed to the greater damage sustained by Houston in Ike compared to Allison. The three P^4v^+ TCs were not included in Figure 25 as two of the three TCs (Hurricanes Charley and Katrina) were rather extraordinary TCs. Insured losses from Hurricanes Charley and Katrina were reported at $7.4 and $40.6 billion respectively. Losses for TS Bonnie were not available from the NHC.

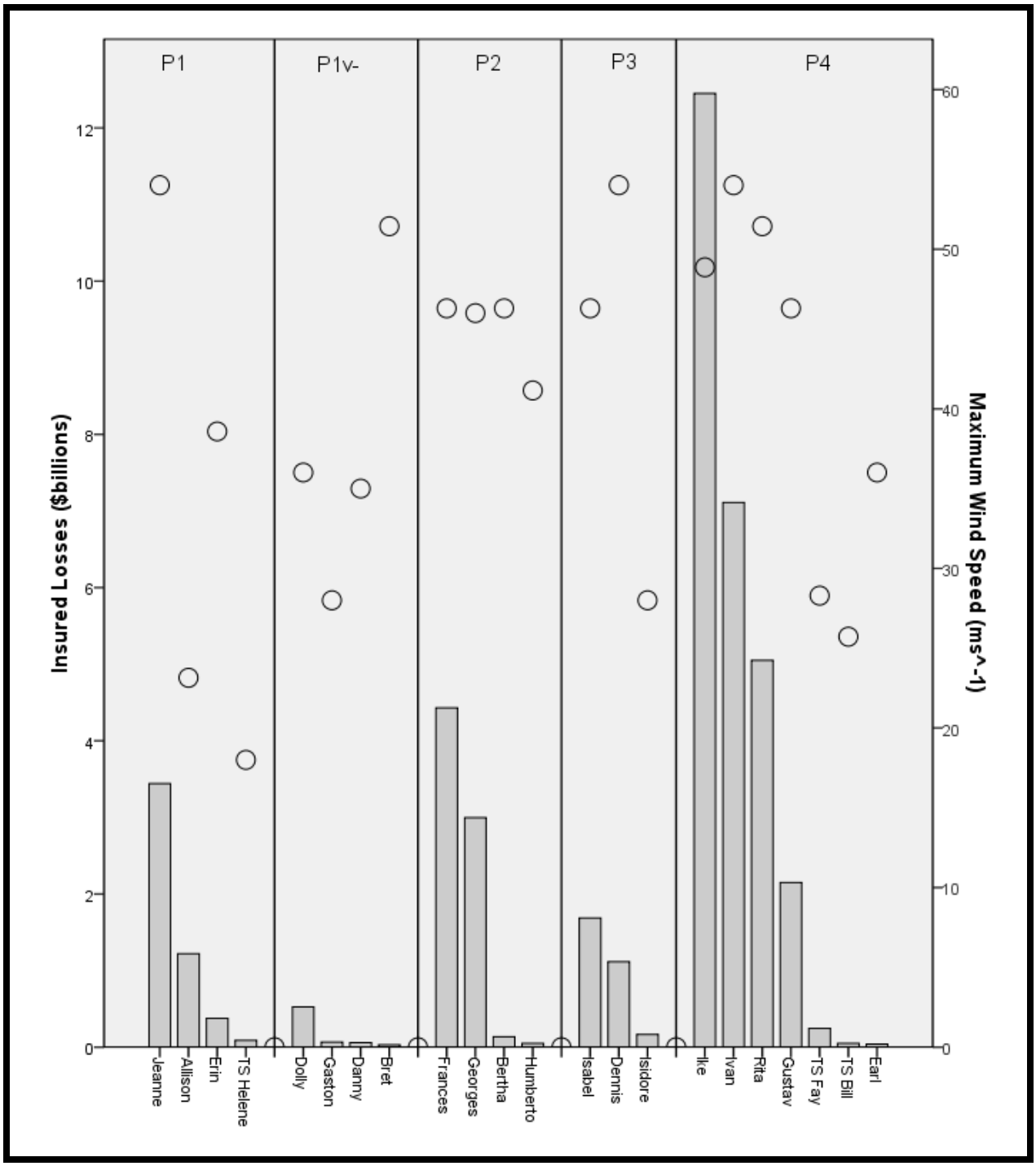

Figure 14: Insured losses (bars) and maximum wind speed at landfall (circles) for each TC as reported by the National Hurricane Center archives. P^4v^+ TCs Charley and Katrina were extreme loss outliers and were omitted from this graphic.

5. Conclusion

The primary goal of this thesis was to categorize land-falling TCs by precipitation characteristics. The author is not aware of any previous research or TC classification scheme that has attempted a similar methodology. Secondary goals were to explore relationships between measures of TC size and rain-shield expansion or dissipation after landfall, and also precipitation intensity. Results are presented in the form of a classification scheme for potential precipitation hazards, ultimately representing hurricane size and translational velocity. The SS scale has proven to be essential for coastal residents in their evacuation decisions and has no doubt saved countless lives since its inception nearly four decades ago. Many studies have been published on attempts to improve (or even retire) the SS scale though that is not the intention of this thesis. Since inland flooding is responsible for more fatalities than any other hurricane hazard, it seems that implementation of a categorical rating system for TC precipitation may prove to be beneficial in warning statements after landfall.

The proposed TCPH scale separates TCs into six discrete types of precipitation storms designed to assess the flooding potential of land-falling TCs. Each type of storm is described by its rain-shield size and, if applicable, a designation of translational velocity: The following is a summary of each of the six types of storms in the TCPH scale.

- Small TCs (P^1)

  Hurricanes Claudette, Erin, and Jeanne made up P^1 TCs, along with tropical storms Allison and Helene. All TCs in this category had rain shields that were below average in size. P^1 TCs contained below average amounts of convective precipitation due to their small size.

- Small TCs with slow translational velocity (P^1v^-)

  P^1v^- TCs share the same precipitation characteristics as P^1 TCs with the distinguishing feature of P^1v^- TCs having a below average forward speed. Translational velocities of P^1v^- TCs were below -

1.00 for three of the four TCs in this group, which consisted of Hurricanes Bret, Danny, Dolly, and Gaston.

- TCs with expanding rain shields (P^2)

  Three of the four TCs in the group had expanding rain shields after landfall; the three that did expand (Hurricanes Bertha, Frances, and Humberto) had positive changes in rain shield area with z-scores > 1.00. Hurricane Georges was approximately the same size at t_{+12} as it was at landfall. P^2 TCs were generally larger than P^1 TCs at landfall and smaller than P^3 TCs (at landfall), which are described below.

- Large TCs (P^3)

  Hurricanes Dennis, Isabel, and Isidore comprised the most homogenous group of TCPH categories. Z-score characteristics for each variables of each TC in this group were quite similar; the one variable that differentiates P^3 TCs from all other groups is the large TC rain shield at landfall. The three TCs in this group also all had little amounts of convective precipitation and rapidly deteriorated after landfall.

- Highly convective TCs (P^4)

  Seven TCs are included in this category, making P^4 TCs the largest group of the TCPH classification scheme. All P^4 TCs had above average amounts of convective precipitation (+40 dBZ). P^4 TCs were also generally larger than average, but all were smaller than P^3 TCs and all were larger than P^1 TCs.

- Fast moving convective TCs with high amounts of convective precipitation (P^4v^+)

  Hurricanes Charley, Katrina, and Tropical Storm Bonnie were considered fast moving TCs with large amounts of convective precipitation as all had larger than average Z-scores for both variables.

This thesis also focused on the variability of rain-shield size and precipitation intensity of TCs. Secondary goals of this thesis were to determine if TCs of similar rain-shield size dissipate uniformly after landfall. This notion was inspired by the observations of rapid wind speed decay associated with high intensity TCs (according to the SS Scale) after landfall. Results suggest that TCs with large rain shields (such as Hurricanes Isabel and Dennis and Tropical Storm Isidore) showed a tendency to rapidly dissipate after landfall while some smaller TCs expanded after landfall, before extratropical transition. There are many variables that are not discussed in this thesis that could influence the expansion or dissipation rates of rain shields. Caution is advised in applying these findings to the prediction of future storms as these tendencies are based on rather limited data due to the present lack of digital data available for analysis.

The classification scheme proposed here is not without its own limitations. The data collection process for this thesis was tedious would be difficult to translate into a real-time operational application. The data collection and processing could become more efficient through better programming techniques; however, for real-time data assimilation the TCPH scale would need to be modified to implement satellite measurements of TC precipitation. The author now has acquired the means to accomplish this, though with the time constraints on completing this M.S. thesis, an improved TCPH scale will be the subject of future work. As of now, it still serves as a viable post-landfall assessment but cannot serve as a forecasting tool like the Saffir-Simpson Scale. If the TCPH scale can be improved and implemented for real-time settings, its use along with the Saffir-Simpson Scale might improve the efficiency and accuracy of emergency management and forecasting statements and warnings.

6. References

Ansari, S., & Del Greco, S. (2005, January 12). GIS tools for visualization and analysis of NEXRAD radar (WSR-88D) archived data at the national climatic data center. San Diego, California.

Arndt, D. S., Basara, B. J., McPherson, R. A., Illston, B. G., McManus, G. D., & Demko, D. B. (2009). Observations of the overland reintensification of Tropical Storm Erin (2007). *Bulletin of the American Meteorological Society* , 1079-1093.

Atallah, E. H., & Bosart, L. F. (2003). The extratropical transition and precipitation distribution of Hurricane Floyd (1999). *Monthly Weather Review , 131*, 1063-1081.

Atallah, E., Bosart, L. F., & Aiyyer, A. R. (2007). Precipitation distribution associated with landfalling tropical cyclones over the eastern United States. *Monthly Weather Review , 135*, 2185-2205.

Baker, E. (1991). Hurricane evacuation behavior. *International Journal of Mass Emergencies and Disasters , 9*, 287-310.

Barnes, G. M., Zipser, E. J., Jorgensen, D., & Marks, J. F. (1983). Mesoscale and convective structure of a hurricane rainband. *Journal of the Atmospheric Sciences , 40*, 2125-2137.

Barnes, G. M., & Stossmeister, G. J. (1986). The structure and decay of of rainband in Hurricane Irene (1981). *Monthly Weather Review , 114*, 2590-2601.

Barnes, G. M., Gamache, J. F., LeMone, M. A., & Stossmeister, G. J. (1991). A convective cell in a hurricane rainband. *Monthly Weather Review , 119*, 776-794.

Bell, K., & Ray, P. S. (2004). North Atlantic hurricanes 1977-1999: Surface hurricane-force wind radii. *Monthly Weather Review , 132*, 1167-1189.

Bosart, L. F., & Bartlo, J. A. (1991). Tropical storm formation in a baroclinic environment. *Monthly Weather Review , 119*, 1971-2013.

Bosart, L. F., & Lackmann, G. M. (1995). Postlandfall tropical cyclone reintensification in a weakly baroclinic environment: A case study of Hurricane David (1979). *Monthly Weather Review , 123*, 3268-3291.

Bove, M. C., Elsner, J. B., Landsea, C. W., Niu, X., & O'Brien, J. J. (1998). Effect of El Nino on U.S. landfalling hurricanes, revisited. *Bulletin of the American Meteorological Society , 79*, 2477-2482.

Brettschneider, B. (2008). Climatological hurricane landfall probability for the United States. *Journal of Applied Meteorology and Climatology , 47*, 704-716.

Burpee, R. W., & Black, M. L. (1989). Temporal and spatial variations of rainfall near the centers of two tropical cyclones. *Monthly Weather Review , 117*, 2204-2218.

Cecil, D. J., Zipser, E. J., & Nesbitt, S. W. (2002). Reflectivity, ice scattering, and lightning characteristics of hurricane eyewalls and rainbands. Part I: Quantitative description. *Monthly Weather Review , 130*, 769-784.

Cerveny, R. S., & Newman, L. E. (2000). Climatological relationships between tropical cyclones and rainfall. *Monthly Weather Review , 128*, 3329-3336.

Crum, T. D., & Alberty, R. L. (1993). The WSR-88D and the WSR-88D operational support facility. *Bulletin of the American Meteorological Society , 74*, 1669-1687.

Dean, L., Emanuel, K. A., & Chavas, D. R. (2009). On the size distribution of Atlantic tropical cyclones. *Geophysical Research Letters , 36*, doi: 10.1029/2009GL039051.

DeMaria, M., & Kaplan, J. (1994). A Statistical Hurricane Intensity Prediction Scheme (SHIPS) for the Atlantic and Eastern North Pacific basins. *Weather and Forecasting , 9*, 209-220.

DeMaria, M., & Kaplan, J. (1999). An updated Statistical Hurricane Intensity Prediction Scheme (SHIPS) for the Atlantic and Eastern North Pacific basins. *Weather and Forecasting , 14*, 326-337.

DeMaria, M., Mainelli, M., Shay, L. K., Knaff, J. A., & Kaplan, J. (2005). Further improvements to the Statistical Hurricane Intensity Prediction Scheme (SHIPS). *Weather and Forecasting , 20*, 531-543.

Demuth, J., DeMaria, M., & Knaff, J. A. (2006). Improvements of advanced microwave sounder unit tropical cyclone intensity and size estimation algorithms. *Journal of Applied Meteorology , 45*, 1573-1581.

Dow, K., & Cutter, S. L. (2000). Public orders and personal opinions: Household strategies for hurricane risk assessment. *Environmental Hazards , 2*, 143-155.

Elsberry, R. L. (2002). Predicting hurricane landfall precipitation: Optimistic and pessimistic views from the Symposium on Precipitation Extremes. *Bulletin of the American Meteorological Society* , 1333-1339.

Elsner, J. B., & Bossak, B. H. (2001). Bayesian analysis of U.S. hurricane climate. *Journal of Climate , 14*, 4341-4350.

Emanuel, K. (2005). *Divine Wind: The History and Science of Hurricanes.* Oxford University Press.

Emanuel, K. (2007). Environmental factors affecting tropical cyclone power dissipation. *Journal of Climate , 20*, 5497-5509.

Emanuel, K. (2003). Tropical cyclones. *Annual Review of Earth and Planetary Sciences , 31*, 75-104.

Garlaneau, T. J., Bosart, L. F., & Schumacher, R. S. (2010). Predecessor rain events ahead of tropical cyclones. *Monthly Weather Review , 138*, 3272-3297.

Goldenberg, S. B., Landsea, C. W., Mestas-Nuñez, A. N., & Gray, W. M. (2001). The recent increase in Atlantic hurricane activity: Causes and implications. *Science , 293*, 474-479.

Gray, W. M. (1984). Atlantic seasonal hurricane frequency. Part I: El Nino and 30 mb Quasi-Biennial Oscillation influences. *Monthly Weather Review , 112*, 1649-1668.

Gray, W. M., Landsea, C. W., Mielke, J. P., & Berry, K. J. (1994). Predicting Atlantic Basin tropical cyclone activity by 1 June. *Weather and Forecasting , 9*, 103-115.

Houze Jr, R. A. (1997). Stratiform precipitation in regions of convection: A meteorological paradox? *Bulletin of the American Meteorological Society* , 2179-2196.

Irish, J. L., Resio, D. T., & Ratcliff, J. J. (2008). The influence of storm size on hurricane surge. *Journal of Physical Oceanography , 38*, 2003-2013.

Jarvinen, B. R., & Caso, E. L. (1978). A tropical cyclone data tape for the north Atlantic basin, 1886-1977: Contents, limitations and uses. 19 pp. National Hurricane Center, 1320 S. Dixie Highway, Coral Gables, FL 33146.

Jordan II, M. R., & Clayson, C. A. (2008). Evaluating the usefulness of a new set of hurricane classification indices. *Monthly Weather Review , 136* (12), 5234-5238.

Jorgensen, D. P. (1984). Mesoscale and convective-scale characteristics of mature hurricanes. Part I: General observations by research aircraft. *Journal of the Atmospheric Sciences , 41*, 1268-1285.

Jorgensen, D. P., & Willis, P. T. (1982). A Z-R relationship for hurricanes. *Journal of Applied Meteorology , 21*, 356-366.

Kalney, E. (1996). The NCEP/NCAR reanalysis 40-year project. *Bulletin of the American Meteorological Society , 77*, 437-471.

Kantha, L. (2006). Time to replace the Saffir-Simpson Scale? *Eos Trans. AGU , 87* (1), doi:10.1029/2006EO010003.

Kaplan, J., & DeMaria, M. (1995). A simple empirical model for predicting the decay of tropical cyclone winds after landfall. *Journal of Applied Meteorology , 34*, 2499-2512.

Kiladis, G. N., & van Loon, H. (1988). The Southern Oscillation. Part VII: Meteorological anomalies over the Indian and Pacific sectors associated with the extremes of the oscillation. *Monthly Weather Review , 116*, 120-136.

Kimball, S. K., & Mulekar, M. S. (2004). A 15-year climatology of North Atlantic tropical cyclones. Part I: Size parameters. *Journal of Climate , 2004*, 3555-3575.

Lewis, B. M., & Jorgensen, D. P. (1978). Study of the dissipation of Hurricane Gertrude (1974). *Monthly Weather Review , 106*, 1288-1306.

Marks, F. D., & Houze, R. A. (1987). Inner core structure of Hurricane Alicia from airborne doppler radar observations. *Journal of the Atmoshperic Sciences , 44*, 1296-1317.

Marks, J. F. (1985). Evolution of the structure of precipitation in Hurricane Allen (1980). *Monthly Weather Review , 113*, 909-930.

Matyas, C. (2007). Quantifying the shapes of U.S. landfalling tropical cyclone rain shields. *The Professional Geographer , 59* (2), 158-172.

Matyas, C. J. (2009). A spatial analysis of radar reflectivity regions within Hurricane Charley (2004). *Journal of Applied Meteorology and Climatology , 48*, 130-142.

Matyas, C. J. (2010). Associations between the size of hurricane rain fields at landfall and their surrounding environments. *Meteorology and Atmospheric Physics , 106*, 135-148.

Maynard, R. H. (1945). Radar and Weather. *Journal of Meteorology , 2*, 214-226.

Medlin, J. M., Kimball, S. K., & Blackwell, K. G. (2007). Radar and rain gauge analysis of the extreme rainfall during Hurricane Danny's (1997) landfall. *Monthly Weather Review , 135*, 1869-1888.

Merrill, R. T. (1984). A comparison of large and small tropical cyclones. *Monthly Weather Review , 112*, 1408-1418.

Moyer, A. C., Evans, J. L., & Powell, M. (2007). Comparison of observed gale radius statistics. *Meteorology and Atmospheric Physics , 97*, 41-55.

National Oceanic and Atmospheric Administration. (2010, February 17). *NOAA National Weather Service to use new hurricane wind scale*. Retrieved February 22, 2010, from http://www.noaanews.noaa.gov/stories2010/20100217_hurricane.html

National Oceanic and Atmospheric Administration. (2005). Doppler radar meteorological observations Part B: Doppler radar theory and meteorology. *Federal Meteorological Handbook no. 11.* 219 pp.

Negri, A. J., Burkhardt, N., Golden, J. H., Halverson, J. B., Huffman, G. J., Larsen, M. C., et al. (2005). The hurricane-flood-landslide continuum. *Bulletin of the American Meteorological Society* , 1241-1247.

Powell, M. D., & Reinhold, T. A. (2007). Tropical cyclone destructive potential by integrated kinetic energy. *Bulletin of the American Meteorological Society* , 513-526.

Rappaport, E. N. (2000). Loss of life in the United States associated with recent Atlantic tropical cyclones. *Bulletin of the American Meteorological Society , 81*, 2065-2073.

Ryan, B. F., Barnes, G. M., & Zipser, E. J. (1992). A wide rainband in a developing tropical cyclone. *Monthly Weather Review , 120*, 431-447.

Senkbeil, J. C., & Sheridan, S. C. (2006). A postlandfall hurricane classification system for the United States. *Journal of Coastal Research , 22*, 1025-1034.

Senkbeil, J. C., Brommer, D. M., Dixon, P. G., Brown, M. E., & Sherman-Morris, K. (2009). The perceived landfall location of evacuees from Hurricane Gustav. *Natural Hazards* .

Senn, H. V., & Hiser, H. W. (1959). On the origin of hurricane spiral bands. *Journal of Meteorology* , 419-426.

Shea, D. J., & Gray, W. M. (1973). The hurricane's inner core region. I. Symmetric and asymmetric structure. *Journal of the Atmospheric Sciences , 30*, 1544-1564.

Shipley, S. T. (2005). GIS applications in meteorology, or adventures in a parallel universe. *Bulletin of the American Meteorological Society* , 171-173.

Simpson, R. H. (1974). The hurricane disaster potential scale. *Weatherwise , 27* (169), 186.

Smith, S. R., Brolley, J., O'Brien, J. J., & Tartaglione, C. A. (2007). ENSO's impact on regional U.S. hurricane activity. *Journal of Climate, 20*, 1404-1414.

Steiner, M., Houze, J. R., & Yuter, S. E. (1995). Climatological characterization of three-dimensional storm structure from operational radar and rain gauge data. *Journal of Applied Meteorology , 34*, 1978-2006.

Trenberth, K. (1997). The definition of El Niño. *Bulletin of the American Meteorological Society , 78* (12), 2771-2777.

Ulbrich, C. W., & Atlas, D. (2002). On the separation of convective and stratiform rains. *Journal of Applied Meteorology , 41*, 188-195.

Weatherford, C. L., & Gray, W. M. (1988). Typhoon structure as revealed by aircraft reconnaissance. Part 1: Data analysis and climatology. *Monthly Weather Review , 116*, 1032-1043.

Willoughby, H. E. (1999). Hurricane heat engines. *Nature , 401*, 649-650.

Willoughby, H. E. (1988). The dynamics of the tropical cyclone core. *Australia Meteorological Magazine , 36*, 183-191.

Appendix A: Weather Surveillance Radar 1988 Doppler Radar Facilities

Identifier	Location	Latitude	Longitude	Elevation (meters)
AKQ	Norfolk, VA	36.98	-77.01	209
AMX	Miami, FL	25.61	-80.41	111
BMX	Birmingham, AL	33.17	-86.77	759
BRO	Brownsville, TX	25.92	-97.42	23
BYX	Key West, FL	24.60	-81.70	89
CAE	Columbia, SC	33.95	-81.12	344
CCX	State College, PA	40.92	-78.00	2,486
CLX	Charleston, SC	32.66	-81.04	211
CRP	Corpus Christi, TX	27.78	-97.51	142
DFX	Laughlin AFB, TX	29.27	-100.28	1,196
DGX	Jackson, MS	32.28	-89.98	609
DIX	Philadelphia, PA	39.57	-74.41	230
EOX	Fort Rucker, AL	31.46	-85.46	499
EWX	Austin, TX	29.70	-98.03	730
GRK	Fort Hood, TX	30.72	-97.38	602
GWX	Columbus AFB, MS	33.90	-88.33	557
GYX	Portland, ME	43.89	-70.26	473
HGX	Houston, TX	29.47	-95.10	115
HTX	Huntsville, AL	34.93	-86.08	1,859
ILN	Cincinnati, OH	39.42	-83.82	1,170
JAX	Jacksonville, FL	30.48	-81.70	130
JGX	Robins AFB, GA	32.67	-83.35	618
LCH	Lake Charles, LA	30.13	-93.22	136
LIX	New Orleans, LA	30.34	-89.83	138
LTX	Wilmington, NC	33.99	-78.43	145
LWX	Sterling, VA	38.98	-77.48	369
LZK	Little Rock, AR	34.84	-92.26	649
MHX	Morehead City, NC	34.78	-76.88	144
MLB	Melbourne, FL	28.11	-80.65	116
MOB	Mobile, AL	30.68	-88.24	289
NQA	Memphis, TN	35.34	-89.87	379
OHX	Nashville, TN	36.25	-86.56	676
OKX	New York City, NY	40.87	-72.86	198
PBZ	Pittsburgh, PA	40.53	-80.22	1,266
POE	Fort Polk, LA	31.16	-92.98	472
RAX	Raleigh, NC	35.66	-78.50	461
RLX	Charleston, WV	38.31	-81.72	1,193
SHV	Shreveport, LA	32.45	-93.84	272

Identifier	Location	Latitude	Longitude	Elevation (meters)
TBW	Tampa Bay, FL	27.70	-82.40	122
VAX	Moody AFB, GA	30.89	-83.00	292
TLH	Tallahassee, FL	30.40	-84.33	176

Appendix B: GIS Program Codes

1.) Add Composite Precipitation Layer

```
Private Sub RadarComposite_Click()
'Set GxDialog
   Dim pGxDialog As IGxDialog
   Set pGxDialog = New GxDialog
   pGxDialog.ButtonCaption = "Add Data"
   pGxDialog.StartingLocation = _
"C:\Documents and Settings\IAN\My Documents\My Stuff\Computer\ArcGIS\School
Files\UA\GY 523\Hurricane Ivan\Precip"
   pGxDialog.Title = "Add Nexrad Radar Data (Composites)"

'***Need a way to add multi-select
   'pGxDialog.AllowMultiSelect = True

   Dim pEnumGxObject As IEnumGxObject

   pGxDialog.DoModalOpen 0, pEnumGxObject
   Dim pGxObject As IGxObject
   Set pGxObject = pEnumGxObject.Next

'If pEnumGxObject Is Nothing Then
 'Needs fixed
'End If

'Get the shapefile workspace
   Dim pWorkspaceFactory As IWorkspaceFactory
   Set pWorkspaceFactory = New ShapefileWorkspaceFactory

   Dim pWorkspace As IWorkspace
   Set pWorkspace = pWorkspaceFactory.OpenFromFile _
      (pGxObject.Parent.FullName, 0)

'Get the shapefile feature class
   Dim pFeatureWorkspace As IFeatureWorkspace
   Set pFeatureWorkspace = pWorkspace

   Dim pFClass As IFeatureClass
   Set pFClass = pFeatureWorkspace.OpenFeatureClass(pGxObject.Name)

'Create a layer
   Dim pFLayer As IFeatureLayer
   Set pFLayer = New FeatureLayer
   Set pFLayer.FeatureClass = pFClass
   pFLayer.Name = pGxObject.Name
```

```
'Set Colors
    Dim pD00 As IRgbColor
    Dim pD0_4 As IRgbColor
    Dim pD5_9 As IRgbColor
    Dim pD10_14 As IRgbColor
    Dim pD15_19 As IRgbColor
    Dim pD20_24 As IRgbColor
    Dim pD25_29 As IRgbColor
    Dim pD30_34 As IRgbColor
    Dim pD35_39 As IRgbColor
    Dim pD40_44 As IRgbColor
    Dim pD45_49 As IRgbColor
    Dim pD50_54 As IRgbColor
    Dim pD55_59 As IRgbColor
    Dim pD60_64 As IRgbColor
    Dim pD65_69 As IRgbColor
    Dim pD70 As IRgbColor

    Set pD00 = New RgbColor
    Set pD0_4 = New RgbColor
    Set pD5_9 = New RgbColor
    Set pD10_14 = New RgbColor
    Set pD15_19 = New RgbColor
    Set pD20_24 = New RgbColor
    Set pD25_29 = New RgbColor
    Set pD30_34 = New RgbColor
    Set pD35_39 = New RgbColor
    Set pD40_44 = New RgbColor
    Set pD45_49 = New RgbColor
    Set pD50_54 = New RgbColor
    Set pD55_59 = New RgbColor
    Set pD60_64 = New RgbColor
    Set pD65_69 = New RgbColor
    Set pD70 = New RgbColor

'Create Colors using RGB code
    pD00.RGB = RGB(204, 204, 204)
    pD0_4.RGB = RGB(204, 204, 204)
    pD5_9.RGB = RGB(190, 210, 255)
    pD10_14.RGB = RGB(115, 178, 255)
    pD15_19.RGB = RGB(0, 92, 230)
    pD20_24.RGB = RGB(163, 255, 115)
    pD25_29.RGB = RGB(76, 230, 0)
    pD30_34.RGB = RGB(56, 168, 0)
    pD35_39.RGB = RGB(255, 255, 0)
    pD40_44.RGB = RGB(255, 170, 0)
    pD45_49.RGB = RGB(255, 85, 0)
    pD50_54.RGB = RGB(255, 0, 0)
```

```
    pD55_59.RGB = RGB(230, 0, 0)
    pD60_64.RGB = RGB(168, 0, 0)
    pD65_69.RGB = RGB(230, 0, 169)
    pD70.RGB = RGB(132, 0, 168)

'Create renderer
    Dim pUVRender As IUniqueValueRenderer
    Set pUVRender = New UniqueValueRenderer

'Fill
    Dim pFill0 As ISimpleFillSymbol
    Set pFill0 = New SimpleFillSymbol
    pFill0.Color = pD00
    pFill0.Outline = Nothing

    Dim pFill1 As ISimpleFillSymbol
    Set pFill1 = New SimpleFillSymbol
    pFill1.Color = pD0_4
    pFill1.Outline = Nothing

    Dim pFill2 As ISimpleFillSymbol
    Set pFill2 = New SimpleFillSymbol
    pFill2.Color = pD5_9
    pFill2.Outline = Nothing

    Dim pFill3 As ISimpleFillSymbol
    Set pFill3 = New SimpleFillSymbol
    pFill3.Color = pD10_14
    pFill3.Outline = Nothing

    Dim pFill4 As ISimpleFillSymbol
    Set pFill4 = New SimpleFillSymbol
    pFill4.Color = pD15_19
    pFill4.Outline = Nothing

    Dim pFill5 As ISimpleFillSymbol
    Set pFill5 = New SimpleFillSymbol
    pFill5.Color = pD20_24
    pFill5.Outline = Nothing

    Dim pFill6 As ISimpleFillSymbol
    Set pFill6 = New SimpleFillSymbol
    pFill6.Color = pD25_29
    pFill6.Outline = Nothing

    Dim pFill7 As ISimpleFillSymbol
    Set pFill7 = New SimpleFillSymbol
    pFill7.Color = pD30_34
```

```
    pFill7.Outline = Nothing

    Dim pFill8 As ISimpleFillSymbol
    Set pFill8 = New SimpleFillSymbol
    pFill8.Color = pD35_39
    pFill8.Outline = Nothing

    Dim pFill9 As ISimpleFillSymbol
    Set pFill9 = New SimpleFillSymbol
    pFill9.Color = pD40_44
    pFill9.Outline = Nothing

    Dim pFill10 As ISimpleFillSymbol
    Set pFill10 = New SimpleFillSymbol
    pFill10.Color = pD45_49
    pFill10.Outline = Nothing

    Dim pFill11 As ISimpleFillSymbol
    Set pFill11 = New SimpleFillSymbol
    pFill11.Color = pD50_54
    pFill11.Outline = Nothing

    Dim pFill12 As ISimpleFillSymbol
    Set pFill12 = New SimpleFillSymbol
    pFill12.Color = pD55_59
    pFill12.Outline = Nothing

    Dim pFill13 As ISimpleFillSymbol
    Set pFill13 = New SimpleFillSymbol
    pFill13.Color = pD60_64
    pFill13.Outline = Nothing

    Dim pFill14 As ISimpleFillSymbol
    Set pFill14 = New SimpleFillSymbol
    pFill14.Color = pD65_69
    pFill14.Outline = Nothing

    Dim pFill15 As ISimpleFillSymbol
    Set pFill15 = New SimpleFillSymbol
    pFill15.Color = pD70
    pFill15.Outline = Nothing

    pUVRender.FieldCount = 1
    pUVRender.Field(0) = "Composite"

'Add Values
    pUVRender.AddValue 0, "-0 dBZ", pFill0
    pUVRender.AddValue 1, "0 dBZ", pFill1
```

```
    pUVRender.AddValue 2, "5 dBZ", pFill2
    pUVRender.AddValue 3, "10 dBZ", pFill3
    pUVRender.AddValue 4, "15 dBZ", pFill4
    pUVRender.AddValue 5, "20 dBZ", pFill5
    pUVRender.AddValue 6, "25 dBZ", pFill6
    pUVRender.AddValue 7, "30 dBZ", pFill7
    pUVRender.AddValue 8, "35 dBZ", pFill8
    pUVRender.AddValue 9, "40 dBZ", pFill9
    pUVRender.AddValue 10, "45 dBZ", pFill10
    pUVRender.AddValue 11, "50 dBZ", pFill11
    pUVRender.AddValue 12, "55 dBZ", pFill12
    pUVRender.AddValue 13, "60 dBZ", pFill13
    pUVRender.AddValue 14, "65 dBZ", pFill14
    pUVRender.AddValue 15, "70+ dBZ", pFill15

    Dim pGFLayer As IGeoFeatureLayer
    Set pGFLayer = pFLayer
    Set pGFLayer.Renderer = pUVRender

'Add the layer to the focus map
    Dim pMxDoc As IMxDocument
    Set pMxDoc = ThisDocument

    pMxDoc.FocusMap.AddLayer pFLayer

    pMxDoc.ActiveView.Refresh
    pMxDoc.UpdateContents
End Sub
```

2.) Union Functions (retain highest reflectivity of overlapping polygons)

```
‘Greatest reflectivity

Dim x As Integer
Dim i As Integer
i = [Category]
Dim ii As Integer
ii = [Category_1]

If i > ii Then
x = i
End If
If ii > i Then
x = ii
End If
If i = ii Then
x = i
```

```
End If
```

3.) Convert Reflectivity Ranges to Single Integers Values

```
Dim x As Integer
If [value] > = 70 Then
x = 15
End If
If [value] < 70 and [value] >= 65 Then
x = 14
End If
If [value] < 65 and [value] >= 60 Then
x = 13
End If
If [value] < 60 and [value] >= 55 Then
x = 12
End If
If [value] < 55 and [value] >= 50 Then
x = 11
End If
If [value] < 50 and [value] >= 45 Then
x = 10
End If
If [value] < 45 and [value] >= 40 Then
x = 9
End If
If [value] < 40 and [value] >= 35 Then
x = 8
End If
If [value] < 35 and [value] >= 30 Then
x = 7
End If
If [value] < 30 and [value] >= 25 Then
x = 6
End If
If [value] < 25 and [value] >= 20 Then
x = 5
End If
If [value] < 20 and [value] >= 15 Then
x = 4
End If
If [value] < 15 and [value] >= 10 Then
x = 3
End If
If [value] < 10 and [value] >= 5 Then
x = 2
End If
```

```
If [value] < 5 and [value] >= 0 Then
x = 1
End If
If [value] < 0 Then
x = 0
End If
```

4.) Sum Stratiform and Convective Precipitation Areas

```
Private Sub SumColumnPrecip_Click()

Dim pMxDoc As IMxDocument
Set pMxDoc = ThisDocument

Dim pFLayer As IFeatureLayer
Set pFLayer = pMxDoc.SelectedItem
Dim pFClass As IFeatureClass
Set pFClass = pFLayer.FeatureClass

Dim pFields As IFields
Set pFields = pFClass.Fields

Dim intAreaIndex As Integer
intAreaIndex = pFields.FindField("F_AREA")

'Filter by radar decibel level
Dim pFilter As IQueryFilter
Set pFilter = New QueryFilter
pFilter.WhereClause = "Composite >= 5"
Dim pFilter2 As IQueryFilter
Set pFilter2 = New QueryFilter
pFilter2.WhereClause = "Composite >= 9"
'Selection Set
Dim pSelectionSet As ISelectionSet
Set pSelectionSet = pFClass.Select(pFilter, _
            esriSelectionTypeHybrid, _
            esriSelectionOptionNormal, Nothing)
Dim pSelectionSet2 As ISelectionSet
Set pSelectionSet2 = pFClass.Select(pFilter2, _
            esriSelectionTypeHybrid, _
            esriSelectionOptionNormal, Nothing)
'Create cursor
Dim pFCursor As IFeatureCursor
Set pFCursor = pFClass.Search(pFilter, True)
Dim pFeature As IFeature
Set pFeature = pFCursor.NextFeature
Dim pFCursor2 As IFeatureCursor
```

```
Set pFCursor2 = pFClass.Search(pFilter2, True)
Dim pFeature2 As IFeature
Set pFeature2 = pFCursor2.NextFeature

Dim dblArea As Double
Dim dblArea2 As Double
Do Until pFeature Is Nothing
   dblArea = dblArea + pFeature.Value(intAreaIndex)
   Set pFeature = pFCursor.NextFeature
Loop
Do Until pFeature2 Is Nothing
   dblArea2 = dblArea2 + pFeature2.Value(intAreaIndex)
   Set pFeature2 = pFCursor2.NextFeature
Loop

'Results
frmResult.Show
frmResult.Caption = "Results Form: " & pFLayer.Name
frmResult.lblResult1.Caption = "Precip Area (km^2)"
frmResult.txtResult1.Text = CStr(dblArea) / 10 ^ 6
frmResult.lblResult2.Caption = "Convective Area (km^2)"
frmResult.txtResult2.Text = CStr(dblArea2) / 10 ^ 6

End Sub
```